MAX-PLANCK-INSTITUT FÜR PLASMAPHYSIK

GARCHING BEI MÜNCHEN

Deduction of Electronic Stopping Coefficients from the Transmission of H^+, D^+ and He^+ through Non-crystalline Gold Foils

János László *, *Wolfgang Eckstein*

Max Planck Institut für Plasmaphysik
D-8046 Garching, FRG
* Alexander von Humboldt fellow at MPI
on leave from Technical University, H-1521 Budapest, Hungary

IPP 9/81 August 1990

Die nachstehende Arbeit wurde im Rahmen des Vertrages zwischen dem Max-Planck-Institut für Plasmaphysik und der Europäischen Atomgemeinschaft über die Zusammenarbeit auf dem Gebiete der Plasmaphysik durchgeführt.

Abstract

An intercomparison between coefficients of low energy, velocity proportional electronic energy loss is presented on the basis of experiments, simulation and an analytical model. The experimental case taken from the literature is the transmission of H^+ , D^+ and He^+ ions through a 590 Å thick polycrystalline Au foil with an initial energy varying between 4 and 17 keV impinging normal to the surface. A version of TRIM.SP is used for the simulation with different built-in electronic energy loss models after the LSS theory, the Andersen and Ziegler compilation, linear response calculations and selfconsistent density functional theory. The analytical model is based on the solution of the classical equation of motion of the projectile. This latter method is proposed for the evaluation of the coefficient of electronic stopping from experimentally determined instantaneous energy values (e.g., the most probable outcoming energy in transmission) in order to achieve comparability between experiment and theory.

Introduction

The present paper proposes a way of deducing the unknown coefficient of low energy, velocity proportional electronic stopping power from experiments. A specific set of transmission experimental results taken from the literature [1] serves as basis of comparison, but other experiments may also be covered as far as they furnish us with the initial energy and an instantaneous energy of ions along their trajectory while penetrating in, or just leaving a solid (e.g., ion scattering). As a special value of instantaneous energy, the most probable outcoming energy of H^+ ,D^+ and He^+ ions transmitted with an initial energy between 4 and 17 keV through a polycrystalline Au foil of 590 Å original thickness is considered for the comparison with Monte Carlo simulation of transmission through an amorphous gold foil of similar thickness. The instantaneous energy of the ions is calculated also analytically solving a newtonian equation of motion of ions regarded as point charges along linear trajectories in the adiabatic limit. The comparison is not presented exclusively for instantaneous energies, but complete measured and simulated transmission energy and emission-angular spectra are compared, too.

Tools

1) Simulation. The TRSPVMC (vectorized version of the TRIM.SP) Monte Carlo code [2] was used to simulate the transmission event. The projectiles are followed along their paths until they stop, be reflected or transmitted through in a series of collision histories.

- Nuclear collisions are described by the incorporated interaction potential proposed by Biersack and Ziegler [3], a fitted analytical formula containing four exponential terms in the screening. This potential is based on the Thomas-Fermi atom model with exchange and correlation contributions. It basicly coincides with the Kr-C potential [4] in the whole radial distance range.

- The low energy velocity proportional electronic stopping based on the LSS calculation [5] is

$$dE/dx_e = NS_e = \frac{\rho L_A}{10^{24} M_2} \frac{8\pi e^2 a_B Z_1^{7/6} Z_2}{(Z_1^{2/3} + Z_2^{2/3})^{3/2}} \frac{v}{v_B} \qquad (1a)$$

namely,

$$dE/dx_e = 0.733 \frac{\rho Z_1^{7/6} Z_2}{M_2 \sqrt{M_1} (Z_1^{2/3} + Z_2^{2/3})^{3/2}} \sqrt{E} = k\sqrt{E} \qquad (1b)$$

with N target atomic density ($Å^{-3}$) and S_e electronic stopping cross section ($eVÅ^2$), ρ target mass density (gcm^{-3}), L_A Avogadro's number, e electron charge ($eV^{1/2}Å^{1/2}$), a_B first Bohr radius (Å), v and v_B projectile and first Bohr velocity ($Ås^{-1}$), resp., Z_1 and Z_2, and M_1 and M_2 projectile and target atomic numbers and masses (these latter in atomic units), resp. E is the instantaneous energy (eV) and k the so called coefficent of friction ($eV^{1/2}Å^{-1}$), then dE/dx_e is given in $eVÅ^{-1}$. For H^+ , D^+ and He^+ the LSS k values are 0.066, 0.047 and 0.071 $eV^{1/2}Å^{-1}$, resp. Note that for such units, the projectile masses are included in the k values.

For the description of the electronic stopping close to the nuclei, an impact parameter dependent loss after Oen and Robinson [6] is built in. An equipartition rule applies then for taking both distant and close interactions into account. It has been shown already [6] that the Oen-Robinson stopping power as a function of energy asymptotically tends to the LSS curve from below with increasing energy. The Oen-Robinson stopping contribution to the inelastic energy loss becomes negligible for only very low energies (about 100 eV). Linear response theory [7] describes also a frictional force like electronic stopping for projectile velocities smaller than the Fermi velocity

$$dE/dx_e = \frac{4m^2e^4}{3\pi\hbar^3}Cv = \frac{0.138}{\sqrt{M_1}}C\sqrt{E} = k\sqrt{E} \qquad (2)$$

with m ($\mathrm{eVs^2\AA^{-2}}$) electron mass, $\hbar$ Planck constant (eVs), C dimensionless constant characteristic to both projectile and target material. For proton-gold interaction, an average k has been determined as 0.089 $\mathrm{eV^{1/2}\AA^{-1}}$(NLG) [8]. Selfconsistent density functional calculations (ENR) [9] result in a k 1.1 times bigger than that for NLG. The Andersen-Ziegler tables (AZ) [10] suggest also velocity proportional stopping for low energy protons. The coefficient is 1.36 times that of LSS.
For helium k is 0.098 $\mathrm{eV^{1/2}\AA^{-1}}$ according to NLG [11], while it is 1.3 times larger for ENR [9]. For AZ [12], k slightly varies with energy (due to the 0.45 power of energy instead of 0.5) around the LSS value. Unfortunately, both the Andersen-Ziegler tables [10] for proton and the Ziegler tables [12] for helium are lacking low energy experimental data for their fitting. These before mentioned coefficients have also been tested in the simulation as well as in the analytical calculation.

2) Analytical Model. Supposing a frozen point charge moving along a linear trajectory in the solid exposed to lose energy due to both electronic and nuclear interactions, we can describe the motion in the adiabatic limit as a simple newtonian. Insisting to the velocity proportional electronic stopping of the form $dE/dx_e = -kE^{1/2}$ (k in $\mathrm{eV^{1/2}\AA^{-1}}$, E in eV and therefore dE/dx_e in $\mathrm{eV\AA^{-1}}$) we can probe different coefficients as described in the previous point for the sake of comparison with experiments and simulation. Concerning the nuclear stopping, we can assume an energy proportional stopping power for H^+ and D^+ , since the energy range in question is well beyond the maximum of the stopping power vs energy function. Unfortunately, for He^+ this holds for energies above 10 keV only. The lines fitted to the nuclear stopping power of the form $dE/dx_n = \alpha E - \beta$ had the following values. $\alpha = 6.923 * 10^{-6}, 1.369 * 10^{-5}, 2.7 * 10^{-5}$ $\mathrm{\AA^{-1}}$, and $\beta = 0.401, 0.797, 3.048$ $\mathrm{eV\AA^{-1}}$ for H^+ , D^+ , He^+ (above 10 keV only), resp. If E is substituted in eV, the stopping power is obtained in $\mathrm{eV\AA^{-1}}$. The equation of motion including both electronic and nuclear stopping contributions is then obtained as

$$x'' + Kx' - A(x')^2 + B = 0 \qquad (3)$$

with $K = k/(2m_1)$ in $\mathrm{s^{-1}}$, if m_1 is the projectile mass in physical units ($\mathrm{eVs^2\AA^{-2}}$), $A = \alpha/2$ in $\mathrm{\AA^{-1}}$ and $B = \beta/m_1$ in $\mathrm{\AA s^{-2}}$. This differential equation can be solved for $x(t)$, $v(t)$, $v(x)$, $E(x)$ and dE/dx (total stopping including both electronic and nuclear contribution) instantaneous quantities in a closed form. (See Appendix A.) These latter

two (via Eq.$A8$ and from $A9$) as a function of travelled pathlength and initial energy, resp. will be compared to the results obtained by direct integration of $dE/dx_n + dE/dx_e$. Direct integration has been numerically performed using the full form of dE/dx_n as described in [13] without the before mentioned linearization (Eq.$B1 - B2$ in Appendix B). The comparison can reveal to what extent the linearization is adequate for the final sections of the trajectories, where the projectile energies fall below the lower limit for the linearization. Direct integration has no restrictions concerning energy, but it can give no account for the time dependence of the projectile motion. In both cases it turns out that the nuclear stopping can be regarded as a perturbation for the initial energies in question, but becomes significant for the slowed-down projectiles.

Methods of Evaluation

In order to get coefficients of the electronic stopping from measured most probable outcoming energies we follow the evaluation widely used by experimentalists , i.e.,

$$k = 2\frac{\sqrt{E_0} - \sqrt{E_1}}{x} \tag{4}$$

by integration of either Eq.1 or 2, where the actual value of x is the layer thickness in Å, E_0 the initial energy and E_1 the instantaneous energy at a depth x, both to be substituted in eV. (We shall refer to this evaluation method as expt1.) Further possibilities are available for this critical evaluation in the literature. In their transmission experiments Blume et al. [1] introduced an average energy of the projectile ($\overline{E}$), that the particles most probably possess in the solid,

$$\overline{E} = \frac{\int_{E_0}^{E_1} E\sqrt{E}dE}{\int_{E_0}^{E_1} \sqrt{E}dE} = \frac{3}{5}\frac{E_0^{5/2} - E_1^{5/2}}{E_0^{3/2} - E_1^{3/2}} \tag{5}$$

for every projectile and every initial energy. Then they accepted a k (for each projectile) belonging to the highest $\overline{E}$, since the k ($\overline{E}$) functions showed saturation at the high energy limit. (This method is referred to as expt2.) Expt3 is a method suggested by Cano [14] on the basis of a finite difference, i.e.,

$$k = \frac{E_0 - E_1}{x\sqrt{E_0}} \tag{6}$$

with x having the actual value of the foil thickness, again. For the sake of comparability, we distinguish between input and output k values in the simulation. The input k 's are those described in the Tools section. The output k 's have been determined on the basis of the most probable simulated outcoming energy according to the different methods of evaluation used in the experiments (Eq.$4 - 6$). These output k values may be considered unphysical, but they still help us to reveal occasional inconsistencies in methods expt1, expt2 and expt3. The analytical method directly results in a k value, if the equation for $E(x)$ (from Eq.$A8$ or Eq.$B1 - B2$) is solved for an unknown K (thus k) substituting a measured or simulated most probable outcoming energy for $E(x)$ at the foil thickness.

Questions to Be Answered

The logic of drawing conclusions from this intercomparison of coefficients of electronic stopping is as follows.

1) With comparing k 's obtained from the same experiment via different methods of evaluation, we can clear up the role of the average energy (E_{av}) value at which the instantaneous electronic stopping is taken, whereas E_{av} is a simple mean value by integrating dE/dx_e between 0 and x and E_0 and E_1 (most probable outcoming energy), or a weighted average ($\overline{E}$), or a finite difference as obtained from expt1, expt2 and expt3, resp. Problems with such simplification of a complete continuous energy loss distribution function to a single mean value have been already discussed to some extent [15].

2) The comparison between input and output k values of the simulation can reveal the importance of the nuclear stopping contribution to the total energy loss. With regard to experimentally determined k 's and simulated output k values, we may attribute the differences to several phenomena not included in the simulation. Such effects are the electronic and nuclear energy loss straggling, skewness and higher moments, the changes in the charge state of the projectile, relativistic effects in the close interactions, different probed target electron densities. Concerning inaccuracies of the experiment [1], we can find the texture effect, namely, that partial channeling can take place in the polycrystalline gold foil (which situation cannot be described with the central symmetrical interaction potential included in both the simulation and the analytical method mentioned in the Tools section), and furthermore, the target thickness as well as the target density may not be even. In addition there can be an absolute error in the original thickness measurement up to 20 %, and an induced surface recession (target thinning) due to sputtering.

3) k 's obtained via the analytical method compared to measured k 's furnish us with information similar to those mentioned in the previous points. The analysis of the relationship between analytically determined and simulated output k 's reveals the difference between energy loss in a friction like picture (motion along a straight line) and in a multiple scattering model. One should take into account here that the travelled pathlengths can be different in the two cases.

Further questions can be answered besides the Z_1 (or rather the M_1) dependence of the transmission spectra regarding not only the peak positions of the measured and simulated spectra, but also the shape of the peaks to find out the role of projectile scattering in off-normal angles (travelling longer paths). Total energy loss vs initial energy functions obtained via transmission experiments, simulation and the analytical method can be compared to results of ion induced secondary kinetic electron yield [16-18] . Finally, the analytical method is proposed to find the electronic stopping coefficient from measured energies at any given point of the linear trajectory of the projectiles.

Results and Discussion

Fig.1a, b and c show the square root of the most probable outcoming energy (E_1 in keV) against the square root of the initial energy (E_0 in keV) for H^+ , D^+ and He^+ projectiles, resp. The different symbols refer to experimental (taken over unchanged from [1]) and simulated results, these latter distinguished by the different theoretical approaches

of the electronic stopping as described in the Tools section (LSS, AZ, NLG, ENR), and the analytical method containing a coefficient of electronic stopping corresponding to the best fitting simulation (achieved by a trial and error method for 17 keV, and referred to as LEV from now on). The bars indicate the influence of a 20 % absolute error allowed for the experimental determination of the original foil thickness. (Lower energy, E_1 corresponds to thicker target.) For proton, the best result could be obtained in the simulation by an electronic stopping coefficient, which was by 7 % larger than the ENR value (in harmony with the estimation in [19]). However, every approach beyond the LSS yielded data within experimental error. For deuterium, LEV could be achieved by an electronic loss coefficient 1.5 times that of LSS. The NLG and ENR values are those obtained for proton divided by the square root of their mass ratio (not included in the figure). AZ data are not available for deuterium. For the case of helium, NLG can be tolerated, ENR furnished us with too low most probable energy values, which fact suggests that the picture of a neutral helium penetrating in amorphous matter may not be an adequate description. LSS and AZ points lay within experimental error. LSS was accepted for LEV. One should, however, note that the statistics of simulation as well as that of the experiment were much worse for He^+ , since more energy entered the target involving many more collision histories. Therefore, the number of escaping projectiles becomes smaller with increasing projectile mass, thicker target and lower initial energy. The lower limit for the number of transmitted per incident projectile was 1 %. The analytical results are in fair agreement with the measured ones. The intersections of the straight lines fitted to the experimental results in [1] with the E_0 axis indicate initial energies, that are fully deposited in the target, namely, projectiles below these limits are absorbed. The off-set is the highest for D^+ , the lowest for H^+ implying a non-negligible projectile mass effect besides the Z_1 effect. The upturn of the experimental values for low impact energies may be due to the following reason.
The experiments were started at high energies and the samples had a restricted area exposable to the primary beam (due to the foil holder), therefore we should not exclude that the foils could be thinned due to sputtering in course of the sequence of measurements. To get an idea about the probability of this induced thickness change, we can make an estimate for the removed layer thickness (Δs, from both surfaces) as follows.

$$\Delta s = v_s t = \frac{\phi_{out} t}{n} = \frac{Y \phi_{in} t}{n} = \frac{Y j t}{ne} = \frac{Y I t}{neA} = \frac{Y I M_2 t}{\rho L_A e A} \qquad (7a)$$

or for the present case

$$\Delta s = 2 * 10^7 \frac{Y I t}{\rho A} \qquad (7b)$$

with v_s sputtering rate, t duration of bombardment, ϕ_{out} and ϕ_{in} outgoing and incoming particle fluxes, resp., n target particle density, Y total sputtering yield (in forward and backward directions), j primary current density, I primary current and A area of the irradiated target surface. If one substitutes I in A, t in s, ρ in gcm^{-3} and A in mm^2, then Eq.7*b* gives the removed layer thickness in Å. Forward, backward and total sputtering yields (number of sputtered particles over the number of incident particles) as a function of primary energy (in keV) are shown in Fig.2a, b and c for H^+ , D^+ and He^+ projectiles, resp. For a typical experimental case $A = 1$ mm^2, $I = 3 * 10^{-10}$ A, which means that the

removal of 100 Å takes approximately 10^7 to 10^9 s. This long must the experiments have not taken, i.e., we can neglect the influence of this effect on our results. It is good to keep in mind, though, that Eq.7*b* gives a lower bound for Δs only.

Normalized measured (taken over unchanged from [1]) and simulated transmitted particle intensities (number of transmitted particles over the number of incident particles) vs energy (keV) of the transmitted H^+ projectiles for some sample cases of 4 to 15 keV incident energies are compared in Fig.3. Note first that the peak positions corresponding to 12 and 15 keV initial energies are too low incosistently with the most probable outcoming energy values in Fig.1 (as displayed in [1]). The factors of normalization (f) are also displayed. The horizontal bar shown as an example on the peak at 12 keV shows the influence of the allowed 20 % tolerance in the foil thickness measurement. (A shift towards lower energies corresponds to a thicker target.) The simulation was done via LEV electronic stopping. (The resolution of the simulated spectra is not better than 1 % of the initial energy, i.e., the energy interval between successive sampling points is $0.01E_0$.) The analytical method results in peak positions within experimental error. It is noteworthy that the widths of the simulated and measured spectra are in agreement unless for low energies, where energy straggling becomes significant and the simulated spectra show almost even distributions (not shown in the figure). For higher energies the peaks have symmetrical, gaussian like shapes. For lower energies a broad low energy shoulder appears. The less expressed tail in the experiment is partly due to the uncorrected measured spetra for a fix energy resolution of the detector, i.e., the experimental values should be divided by energy at each energy. Another reason is that only a small fraction of ions can get through the target without change in the charge state, namely without capturing an electron. Since the capture cross section steeply increases with decreasing energy [20], the majority of projectiles are neutralized very probably in a duration one or two orders of magnitude smaller than the total time of flight. This estimate is done for bulk aluminium, though [20].

For our case Fig.4 shows the time of flight in units of 10^{-15} s against the travelled linear depth (in Å) for the sample case of H^+ penetrating in gold for two different initial energies and two different values of the coefficient of electronic stopping. Solid and dashed line correspond to LEV and LSS coefficients, resp. The curves all start at zero and terminate, when and where the projectiles loose their energy. This calculation has been obtained by a linearized nuclear stopping power. For H^+ , the linearization of the nuclear stopping does not play a visible role in the dynamic description as compared to the full nuclear stopping.

Returning to our main stream of charge exchange processes, and assuming that only survived or reionized charge are detected, the neutral background spectra for low energies would surpress the peaks seen in Fig.3 completely. The density functional formalism results in an energy loss dependence on energy for neutrals similar to that of the linear response theory for frozen charges [21]. It would be then reasonable to get simulated low energy peaks, but the measured peaks could not be attributed to such a bulk energy loss process, since the ionization of the measured ions happens very likely at the exit surface (within 10^{-15} s as estimated from the capture cross section of He scattering on Al from [9]). The spectra are taken with a small angular acceptance around the surface normal. The low energy shoulders are responsible that the expected value of the transmitted energy distribution is

always lower than the most probable outcoming energy attributed to the maximum. For H^+ , D^+ and He^+ projectiles, the ratios of the most probable outcoming energy and the maximum energy vary between 0.71 and 0.87, 0.75 and 0.91 and 0.75 and 0.78, resp. approaching unity with increasing energy.

Fig.5a and b display a detailed example of a transmitted energy spectrum (number of transmitted particles over the number of incident particles) vs energy (keV) of transmitted protons of 17 keV initial energy as measured (taken over unchanged from [1]), simulated and analytically determined, resp. parametrized by the polar emission angle (final scattering angle) shown in the insert. Simulation and the analytical point have been obtained via LEV. The bars show again the uncertainty due to the inaccuracy of the thickness measurement. (Lower peak position corresponds to thicker target.) The spectra are normalized to unity. Note that with increasing polar angle the most probable outcoming energy shifts towards lower energies according to the fact, that the projectiles escaping under oblique angles must have travelled longer paths, i.e., they had more chance to lose their energy. The statistics becomes poorer with increasing polar angle. The analytical point agrees well with the peak position.

Fig.6 is a compilation of k values (in units of $eV^{1/2}Å^{-1}$) as a function of energy (keV). Fig.6a, b and c show results for H^+ , D^+ and He^+ , resp. Different symbols denote different theoretical approaches for the input k values (LSS, AZ, etc), and the analytical points. Note that the illustrated k 's are output values (the corresponding input k 's are shown by the horizontal lines) resulted by the simulation after many possible projectile histories. It is instructive to observe that the input k values are lower limits of the output k 's (as evaluated via expt1) in the high energy regime. This has to do with either the nuclear energy loss included in the simulation and contributing more and more to the total loss as the instantaneous energy of the projectiles decreases, or it means that the evaluation methods do not work properly, or both. Table 1 is a collection of rounded $\Delta E_e/\Delta E_n$ (electronic per nuclear energy loss of transmitted projectiles) obtained via LEV simulation. The measured k values have a break down for low average energies [1], which contradicts to our physical picture as well as to Eq.4. If we do not consider transmitted projectiles in tilted angles, we restrict ourselves by excluding nuclear stopping contribution to the energy loss, i.e., we consider projectiles that have travelled the shortest pathlengths (projected instead of average range), and in addition we probe a metallic electron density lower than the average. This leads to an overestimation of k 's and thus that of the electronic energy loss by a factor of 1.1-1.2. Table 2 is a compilation of simulated k values ($eV^{1/2}Å^{-1}$) determined as input (for different theoretical approaches) and output values evaluated via all three expt1, expt2 and expt3 methods. Note the above mentioned high values for the lowest energies. The ignored nuclear loss contribution changes the mean k value (increases it) suggesting that none of expt1, expt2 and expt3 apply, even if they would be correct for targets of finite thicknesses.

A more detailed illustration of k values ($eV^{1/2}Å^{-1}$) against emission angle for 13 keV H^+ and He^+ projectiles is presented in Fig.7a and b, resp. Different symbols correspond to different input k values again. The bars denote deviations due to the allowed 20 % error in the thickness measurement (lower k is attributed to thinner target). These k values have been corrected for the different pathlengths [1]. Namely, an arithmetic mean of x and

$x/cos\vartheta$

$$\overline{x} = \frac{x}{2}(1 + \frac{1}{\cos\vartheta}) \tag{8}$$

effective thickness has been substituted for x in Eq.4 (expt1), where ϑ is the emission angle. The correction aligns the k values and moves them systematically closer to the stable (input) values giving evidence that the cosine distribution can be an adequate description. Remember that the measured k values are too high due to the evaluation used (expt2 in this case).

The analytical model is also applicable to present instantaneous energy of the projectiles moving in the solid. Fig.8a, b and c show energy degradation of H^+ , D^+ and He^+ projectiles, resp. vs travelled pathlength in gold. The starting points indicate the initial energies, while depths, where the curves vanish correspond to thicknesses of gold with the capability to absorb the projectile. Solid lines denote results with LEV coefficient of electronic stopping, dashed lines are attributed to other coefficients. A full form of the nuclear stopping has been considered. The gradients of these curves (namely, the instantaneous energy losses) are greater by the entrance of the projectiles (this stays hidden in the logarithmic depth scaling, see the linearly scaled insert in Fig.8a), which fact forwards us the message that the energy square root depending electronic energy loss is dominant at these higher energies. At farther depths the energy functions become less steep, slowing-down and energy deposition proceed, and the energy proportional nuclear stopping overtakes the governing role.

Fig.9a, b and c display electronic stopping power ($eV\AA^{-1}$) vs initial energy (keV) for H^+ , D^+ and He^+ projectiles, resp. For H^+ and D^+ the nuclear energy losses are small even for low energies (see Table 1). However, for He^+ the nuclear loss contribution is significant. The upward arrows in Fig.9c show shifts, that have been obtained by taking not only electronic, but nuclear energy losses into account, too. The bars in the figures denote the effect of uncertain foil thickness again (smaller loss corresponding to thinner target). The analytical curves are based on a full nuclear stopping contibution. Not only the experimental points of [1] (unconnected dots), but data deduced from kinetic secondary electron emission yield measurements [16,17,18] (dots connected by dotted, dashed-dotted and dashed lines, resp.) are displayed in the figure, too. The kinetic secondary electron yield is proportional with the electronic energy loss ($\gamma = \Lambda dE/dx_e$). If we take Λ=0.108, 0.197 and 0.112 $\AA eV^{-1}$ for H^+ , D^+ and He^+ , resp., by fitting the electronic energy losses at 17 keV, we find a convincing coincidence between measured and calculated electronic loss functions. The fitted Λ values are in agreement with published data [22]. The analytical curves lay well below the experimental data owing partly to the inadequate experimental evaluation of the raw data leading to an average energy loss rather than to an instantaneous one. In comparison with the simulated results we should admit that the rudeness of the analytical model, first of all the assumption of a linear trajectory allows farther penetration of the projectiles, consequently becomes responsible for the lower energy loss.

The description of a charged particle moving along a straight line in an electron gas is based, e.g., on transmission experiments in channeling directions of single crystals [1,22]. One would expect higher k values for polycrystalline and amorphous materials. This fact has been justified from both experimental and theoretical aspects in earlier

works [1,8,19] and is verified in the present paper, too. The good agreement between measured and analytically determined most probable outcoming energies suggests us that the projectile motion in the solid can be properly described by the decelerated motion due to electronic and nuclear stopping, i.e., the multiple scattering model can be saved for angular distribution examinations. (Such investigations can also be characterized by the analytical model assuming, e.g., a cosine pathlength distribution.) Concerning the evaluation methods (Eq.4 – 6) shown not to give reasonable results, the application of the analytical model is recommended as an easy way of finding the coefficient of electronic stopping as discussed in the Methods of Evaluation section. For transmission experiments, the analytical method results in about the same k values as the simulation with LEV electronic stopping.

Assuming that target electrons of the range of metallic electron densities (with a one electron radius between 0.5 and 1.6 Å) respond similarly to the penetration of light ions (as suggested from both linear response and density functional theories), we can make a prediction for the appropriate coefficient of electronic stopping as compared to the LSS value. Data compiled in Table 3 are LSS (input) k values of amorphous targets of metallic electron densities [23] multiplied by a correction factor calculated for gold, i.e., 1.6, 1.5 and 1.0 for H^+ , D^+ and He^+ projectiles, resp. Similar data from the Andersen and Ziegler [10] and Ziegler [12] tables are also listed for the sake of comparison (for the case of helium only for initial energies below 10 keV and, for average energies between 0.5 and the actual power of energy [12]). Obviously enough Z_2 oscillations as predicted by the LSS theory are preserved.

Conclusions

The authors succeeded in achieving reasonable agreement concerning several quantities (most probable outcoming energy, energy and angular spectra, deduced stopping powers of low energy light projectiles transmitted through gold foils) between their Monte Carlo simulation and experiments taken from the literature. An increased electronic loss was found for H^+ and D^+ projectiles in amorphous matter compared to single crystalline targets. The LSS stopping had to be modified by a factor of 1.6 and 1.5 for H^+ and D^+ projectiles, respectively, while it remained unchanged for He^+ . A handy, analytical calculation is recommended for the evaluation of the coefficients of electronic stopping for experimentalists.

Acknowledgement

J.L. is indebted to Dr.H.Verbeek for his cooperation in this paper, and he appreciates inspiring discussions with Prof.F.Flores and with Dr.I.Nagy.

Appendix A

In the energy range in question, the nuclear and the electronic stopping power can be described as

$$dE/dx_n = \alpha E - \beta = \alpha' v^2 - \beta \qquad (A1)$$

and

$$dE/dx_e = -kE^{1/2} = -k'v \qquad (A2)$$

resp. The newtonian equation of motion of a frozen point charge moving along a straight line and exposed to energy loss due to both nuclear and electronic interaction with the medium is then obtained

$$x'' + Kx' - A(x')^2 + B = 0 \qquad (A3)$$

with $K = k'/m_1 = k/(2m_1)^{1/2}$ in s^{-1}, $A = \alpha'/m_1 = \alpha/2$ in $Å^{-1}$, $B = \beta/m_1$ in $Ås^{-2}$, if k is in $eV^{1/2}Å^{-1}$, α in $Å^{-1}$ and β in $eVÅ^{-1}$, and m_1 is the projectile mass in physical units ($eVs^2Å^{-2}$).

The initial conditions for this second order, nonlinear, inhomogeneous, separable ordinary differential equation are $t(0) = 0$ (s), $x(0) = 0$ (Å), $dx/dt(0) = v_0$ ($Ås^{-1}$). We substitute v for dx/dt first, and solve the first order equation for $v(t)$ instantaneous velocity ($Ås^{-1}$) by separating the variables, and integrating from 0 to t in time (from v_0 to v in velocity).

$$v(t) = \frac{\Delta^{1/2}/A}{1 - \frac{2Av_0 - K - \Delta^{1/2}}{2Av_0 - K + \Delta^{1/2}} exp(-\Delta^{1/2}t)} + \frac{K - \Delta^{1/2}}{2A} \qquad (A4)$$

with $\Delta = K^2 + 4AB$ (s^{-2}). We can now solve Eq.$A4$ by for $x(t)$ instantaneous travelled pathlength (Å) separating the variables and integrating from 0 to t in time (from 0 to x in distance).

$$x(t) = \frac{K - 3\Delta^{1/2}}{2A}t - \frac{1}{A}\ln[1 - \frac{2Av_0 - K - \Delta^{1/2}}{2Av_0 - K + \Delta^{1/2}}\exp(-\Delta^{1/2}t)] + \ln\frac{2\Delta^{1/2}}{2Av_0 - K + \Delta^{1/2}} \qquad (A5)$$

(An actual value of $x(t)$ can be the foil thickness in transmission.) We can now express $t(x)$ (in s) from Eq.$A5$ by expanding $x(t)$ in a McLaurin series of second order.

$$t(x) \approx \frac{v_0 - K/A + \Delta^{1/2}/A - [(v_0 - K/A + \Delta^{1/2}/A)^2 - (Av_0^2 - Kv_0 - AB)x]^{1/2}}{Av_0^2 - Kv_0 - AB} \qquad (A6)$$

The motion of the particle is finished, the particle is stopped, if the determinant in Eq.$A6$ becomes nonpositive. Therefore the maximum projected range (Å) is

$$x_{max} = \frac{(v_0 - K/A + \Delta^{1/2}/A)^2}{Av_0^2 - Kv_0 - AB} \qquad (A7)$$

Substituting $t(x)$ back into Eq.$A4$, we get $v(x)$ instantaneous velocity ($Ås^{-1}$) as a function of the travelled pathlength

$$v(x) = \frac{\Delta^{1/2}/A}{1 - \frac{2Av_0 - K - \Delta^{1/2}}{2Av_0 - K + \Delta^{1/2}} exp[-\Delta^{1/2}t(x)]} + \frac{K - \Delta^{1/2}}{2A} \qquad (A8)$$

$E(x)$ instantaneous kinetic energy of the projectile is then $E(x) = \frac{1}{2} m_1 v(x)^2$ (in eV) and dE/dx instantaneous total energy loss per pathlength (eVÅ^{-1}) is

$$dE/dx = \frac{mv(x)^2[v(x) - \Delta^{1/2}/A]}{[(v_0 - K/A + \Delta^{1/2}/A)^2 - (Av_0^2 - Kv_0 - AB)x]^{1/2}} \tag{A9}$$

which is a rather complicated, but purely algebraic implicit function of the initial energy and the pathlength.

If the nuclear energy loss contribution is negligible, i.e., $\alpha = 0$ and $\beta = 0$, then the instantaneous velocity as a function of initial velocity and pathlength is

$$v(x) = v_0 \exp[(1 - \frac{2Kx}{v_0})^{1/2} - 1] \tag{A10}$$

Eq.$A10$ is the sum of the following infinite McLaurin series

$$v(x) = v_0 - \sum_{i=1}^{\infty} \frac{(Kx)^i}{i!} \tag{A11}$$

The first order expansion of this series satisfies the solution proposed earlier [8].

Appendix B

The numerical solution of the integration of dE/dx involves the full form of dE/dx_n as proposed in [13]

$$dE/dx_n = 0.4231 \frac{Z_1 Z_2 M_1 N}{(M_1 + M_2)(Z_1^{2/3} + Z_2^{2/3})^{1/2}} * G \tag{B1}$$

where

$$G = \frac{\log(1 + \epsilon)}{\epsilon + 0.10718\epsilon^{0.37544}}$$

and

$$\epsilon = 0.03253 \frac{M_2 E}{Z_1 Z_2 (M_1 + M_2)(Z_1^{2/3} + Z_2^{2/3})^{1/2}}$$

E to be substituted in eV, N in Å^{-3}, M_1 and M_2 in atomic units to get dE/dx_n in eVÅ^{-1}. We obtain

$$\int_E^{E_0} \frac{dE'}{f(E')} = \int_0^x dx' \tag{B2}$$

and

$$f(E') = dE/dx_n(E') + dE/dx_e(E')$$

Namely, the unknown instantaneous energy value E appears in the lower limit of the integral for a given value of E_0 initial energy and x travelled depth. Therefore one has to find the root of Eq.$B2$. The iterative approach for the root (a slowly converging, but exact interval halving method was applied) implies the successive evaluation of the integral with the argument $f(E')$. The evaluation of the integral can be executed by a Gaussian quadrature. With the help of the following transformation

$$E' = \frac{E_0 - E}{2}\xi + \frac{E_0 + E}{2} \tag{B3}$$

Eq.$B3$ becomes

$$\frac{E_0 - E}{2}\int_{-1}^{+1} f(E')d\xi \tag{B4}$$

to be approximated by

$$\frac{E_0 - E}{2}\sum_{i=1}^{n} a_i f(\frac{E_0 - E}{2}b_i + \frac{E_0 + E}{2}) \tag{B5}$$

with the weights and abscissas from e.g., [24].

References

1 R.Blume, Thesis, Ludwig Maximilians Universität, München, 1980,
R.Blume, W.Eckstein, H.Verbeek, Nucl.Instr.Meth. 168 (1980) 57,
R.Blume, W.Eckstein, H.Verbeek, K.Reichelt, Nucl.Instr.Meth. 194 (1982) 67.

2 R.Aratari, W.Eckstein, Nucl.Instr.Meth. B42 (1989) 11.

3 J.P.Biersack, J.F.Ziegler, Nucl.Instr.Meth. 194 (1982) 93.

4 W.D.Wilson, L.G.Haggmark, J.P.Biersack, Phys.Rev. B15 (1977) 2458.

5 J.Lindhard, M.Scharff, H.E.Schiott, K.Dan.Vidensk.Selsks.Mat-Fys.Medd. 33/14 (1963).

6 O.S.Oen, M.T.Robinson, Nucl.Instr.Meth. 132 (1976) 647.

7 E.Fermi, E.Teller, Phys.Rev. 72 (1947) 399,
B.A.Trubnikov, Yu.N.Yavlinskii, Zh.Eksp.Teor.Fiz. 48 (1965) 253,
J.Lindhard, A.Winther, K.Dan.Vidensk.Sesks.Mat-Fys.Medd. 34/4 (1964).

8 I.Nagy, J.László, J.Giber, Z.Phys. A321 (1985) 221.

9 P.M.Echenique, R.M.Nieminen, R.H.Ritchie, Solid State Comm. 37 (1981) 779,
M.J.Puska, R.M.Nieminen, Phys.Rev. B27 (1983) 6121.

10 H.H.Andersen, J.F.Ziegler, Stopping Powers and Ranges in All Elements, Vol.3, Pergamon Press, N.Y., 1977.

11 I.Nagy, J.László, J.Giber, Nucl.Instr.Meth. B27 (1987) 276.

12 J.F.Ziegler, Stopping Powers and Ranges in All Elements, Vol.4, Pergamon Press, N.Y., 1977.

13 J.F.Ziegler, Stopping Cross-Sections for Energetic Ions in All Elements, Vol.5, Pergamon Press, N.Y., 1980.

14 G.L.Cano, J.Appl.Phys. 43 (1972) 1504.

15 J.László, J.Phys. F17 (1987) 893.

16 G.Lakits, F.Aumayr, H.Winter, Europhys.Lett. 10 (1989) 679.

17 P.C.Zalm, L.J.Beckers, Philips J.Res. 39 (1984) 61.

18 R.A.Baragiola, E.V.Alonso, A.Oliva-Floria, Phys.Rev. B19 (1979) 121.

19 I.Nagy, A.Arnau, P.M.Echenique, Phys.Rev. A40 (1989) 987.

20 P.M.Echenique, F.Flores, R.H.Ritchie, Solid State Physics, Vol.43 (1990) 229.

21 P.M.Echenique, I.Nagy, A.Arnau, Int.J.Quant.Chem.: Quant.Chem.Symp. 23 (1989) 521.

22 D.Hasselkamp, K.G.Lang, A.Scharmann, N.Stiller, Nucl.Instr.Meth. 180 (1981) 349.

23 J.F.Ziegler, J.P.Biersack, U.Littmark, The Stopping and Range of Ions in Solids, Vol.1, Pergamon Press, N.Y., 1985, pp.223.

24 G.A.Korn, T.M.Korn, Mathematical Handbook for Scientists and Engineers, McGraw-Hill, N.Y., 1961, pp.664.

Tables

Table 1) *Collection of rounded $\Delta E_e/\Delta E_n$ values (electronic over nuclear energy loss of H^+ , D^+ and He^+ ions transmitted through gold foils) obtained via LEV simulation. (Negative signs stand for unavailable data.)*

projectile	initial energy (keV)						
	4	5	8	12	13	15	17
H^+	39	-	59	82	85	91	108
D^+	-	15	20	-	28	-	36
He^+	4	-	5	-	7	-	8

Table 2) *Collection of k values ($eV^{1/2}Å^{-1}$) determined as input and as output values from the experiment [1] (via three ways of evaluation expt1, expt2 and expt3) and on the basis of different theories of the electronic stopping (as described in the Tools section) for H^+ , D^+ and He^+ transmission through gold foils. (Negative signs stand for data not available.)*

projectile	theory or exp.	input	output							
			initial energy (keV)							
			4	8	11	12	13	15	17	average
H^+	LSS	0.066	0.105	0.074	-	-	0.070	0.070	0.070	0.078
	NLG, AZ	0.089	-	0.100	0.099	-	0.100	0.094	0.097	0.098
	PN	0.099	-	0.116	-	-	0.110	-	0.102	0.109
	LEV	0.106	0.147	0.119	-	0.117	0.113	0.110	0.111	0.120
	exp1	-	0.097	0.121	0.116	0.125	0.122	0.128	0.110	0.117
	exp2	-	-	-	-	-	-	-	-	0.128
	exp3	-	0.075	0.097	0.097	0.104	0.103	0.108	0.096	0.097
			4	5	8	13	17	average		
D^+	LSS	0.047	0.064	0.057	0.053	0.050	0.049	0.055		
	LEV	0.071	-	0.094	0.082	0.075	0.075	0.082		
	exp1	-	-	0.067	0.075	0.081	0.080	0.077		
	exp2	-	-	-	-	-	-	0.091		
	exp3	-	-	0.058	0.066	0.073	0.073	0.069		
			4	8	13	17	average			
He^+	LSS, AZ	0.071	0.147	0.111	0.085	0.080	0.106			
	NLG	0.098	-	-	0.119	0.120	0.120			
	PN	0.116	-	-	0.139	0.133	0.136			
	LEV	0.071	0.147	0.111	0.085	0.080	0.106			
	exp1	-	-	0.099	0.101	0.101	0.101			
	exp2	-	-	-	-	-	0.117			
	exp3	-	-	0.084	0.088	0.090	0.087			

Table 3) *LSS, AZ and LEV k values* ($eV^{1/2}Å^{-1}$) *for* H^+ , D^+ *and* He^+ *projectiles moving in amorphous targets of metallic electron densities* [23]. *(Negative signs stand for data not available.)*

target	projectile								
	H^+			D^+			He^+		
	LSS	AZ	LEV	LSS	AZ	LEV	LSS	AZ	LEV
Li	0.031	0.021	0.050	0.022	-	0.033	0.027	0.020	0.027
Be	0.089	0.085	0.142	0.063	-	0.094	0.079	0.086	0.079
B	0.103	0.102	0.164	0.072	-	0.109	0.093	0.126	0.093
C	0.093	0.095	0.149	0.066	-	0.099	0.086	0.119	0.086
Na	0.023	0.020	0.038	0.017	-	0.025	0.023	0.052	0.023
Mg	0.040	0.052	0.065	0.029	-	0.043	0.040	0.055	0.040
Al	0.057	0.079	0.091	0.040	-	0.061	0.056	0.063	0.056
Si	0.048	0.065	0.076	0.034	-	0.051	0.047	0.046	0.047
K	0.013	0.022	0.021	0.009	-	0.014	0.013	0.028	0.013
Ca	0.023	0.040	0.037	0.016	-	0.025	0.024	0.042	0.024
Ti	0.058	0.087	0.092	0.041	-	0.061	0.059	0.086	0.059
V	0.074	0.102	0.118	0.052	-	0.078	0.075	0.126	0.075
Cr	0.086	0.105	0.137	0.060	-	0.091	0.088	0.149	0.088
Mn	0.084	0.089	0.134	0.059	-	0.089	0.086	0.132	0.086
Fe	0.088	0.094	0.141	0.062	-	0.093	0.090	0.126	0.090
Co	0.093	0.089	0.150	0.066	-	0.099	0.096	0.121	0.096
Ni	0.095	0.103	0.152	0.067	-	0.101	0.098	0.122	0.098
Cu	0.089	0.099	0.142	0.063	-	0.094	0.092	0.088	0.092
Zn	0.069	0.087	0.110	0.049	-	0.073	0.071	0.068	0.071
Ga	0.054	0.081	0.086	0.038	-	0.057	0.056	0.053	0.056
Ge	0.047	0.078	0.075	0.033	-	0.050	0.049	0.075	0.049
As	0.049	0.077	0.078	0.034	-	0.052	0.051	0.055	0.051
Se	0.039	0.068	0.062	0.027	-	0.041	0.040	0.055	0.040
Rb	0.012	0.019	0.018	0.008	-	0.012	0.012	0.031	0.012
Sr	0.019	0.036	0.031	0.014	-	0.020	0.020	0.039	0.020
Zr	0.046	0.091	0.074	0.033	-	0.049	0.048	0.122	0.048
Mo	0.069	0.130	0.111	0.049	-	0.073	0.073	0.157	0.073
Pd	0.074	0.112	0.118	0.052	-	0.078	0.078	0.122	0.078
Ag	0.064	0.104	0.102	0.045	-	0.068	0.067	0.101	0.067
Cd	0.050	0.084	0.080	0.035	-	0.053	0.053	0.065	0.053
In	0.042	0.076	0.067	0.030	-	0.044	0.044	0.057	0.044
Sn	0.040	0.075	0.065	0.029	-	0.043	0.043	0.067	0.043
Sb	0.036	0.078	0.057	0.025	-	0.038	0.038	0.057	0.038
Te	0.032	0.065	0.052	0.023	-	0.034	0.034	0.046	0.034
Cs	0.009	0.020	0.015	0.007	-	0.010	0.010	0.031	0.010
Ba	0.017	0.039	0.027	0.012	-	0.018	0.018	0.049	0.018

Ta	0.062	0.083	0.099	0.044	-	0.066	0.066	0.118	0.066
W	0.071	0.091	0.113	0.050	-	0.075	0.076	0.122	0.076
Pt	0.074	0.093	0.119	0.052	-	0.079	0.080	0.103	0.080
Au	0.066	0.091	0.106	0.047	-	0.070	0.071	0.073	0.071
Tl	0.039	0.052	0.063	0.028	-	0.042	0.042	0.059	0.042
Pb	0.037	0.055	0.059	0.026	-	0.039	0.040	0.067	0.040
Bi	0.032	0.053	0.051	0.023	-	0.034	0.034	0.075	0.034

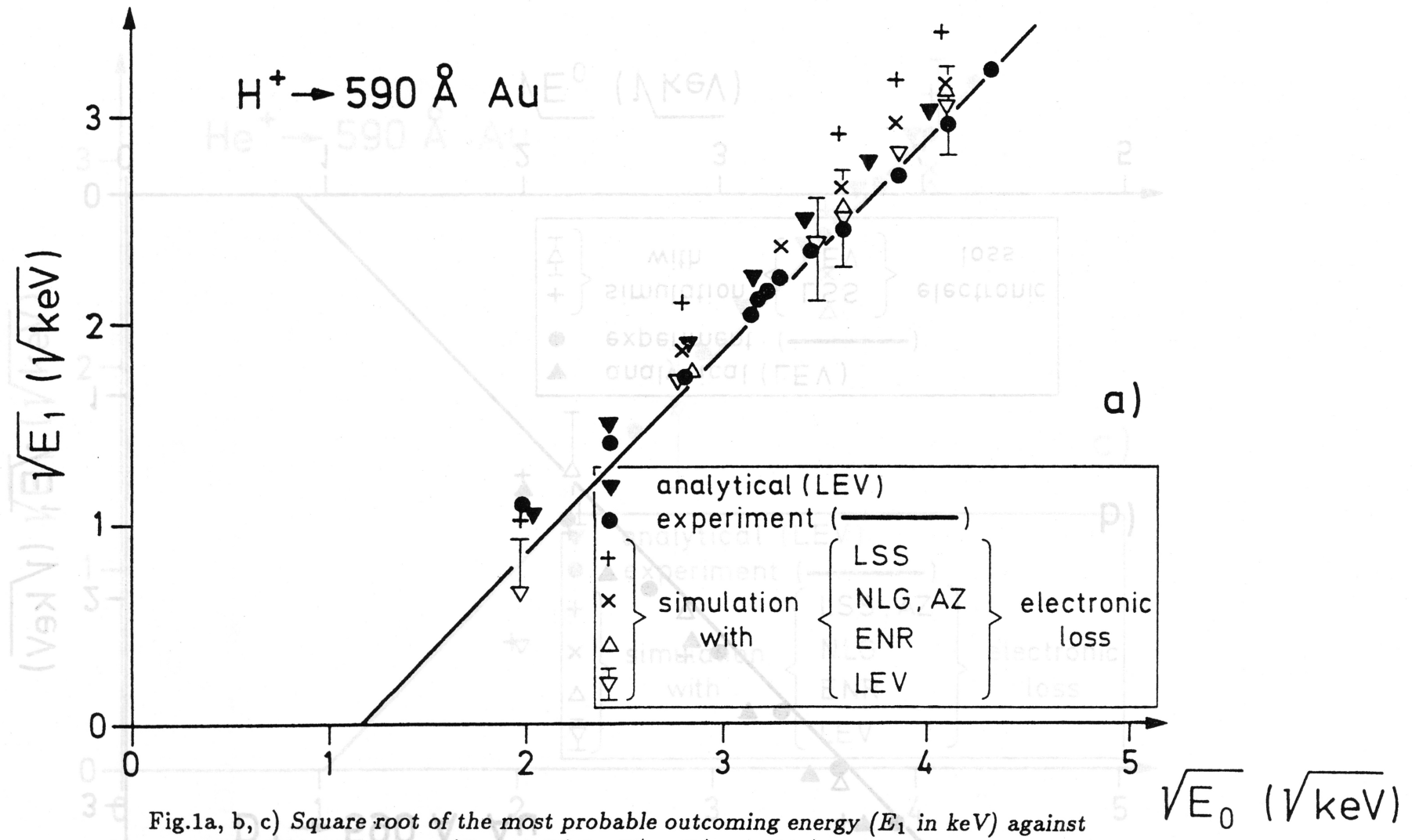

Fig.1a, b, c) *Square root of the most probable outcoming energy (E_1 in keV) against the square root of initial energy (E_0 in keV) for H^+ , D^+ and He^+ projectiles transmitted through Au foils, resp. The different symbols refer to experimental [1], analytical and simulated results, these latter distinguished by the different theoretical approach of the electronic energy loss as described in the Tools section. The bars indicate the influence of a 20 % absolute error allowed for the determination of the initial foil thickness measurement. (Lower energy corresponds to thicker target.) Solid lines are fitted to the experimental values [1].*

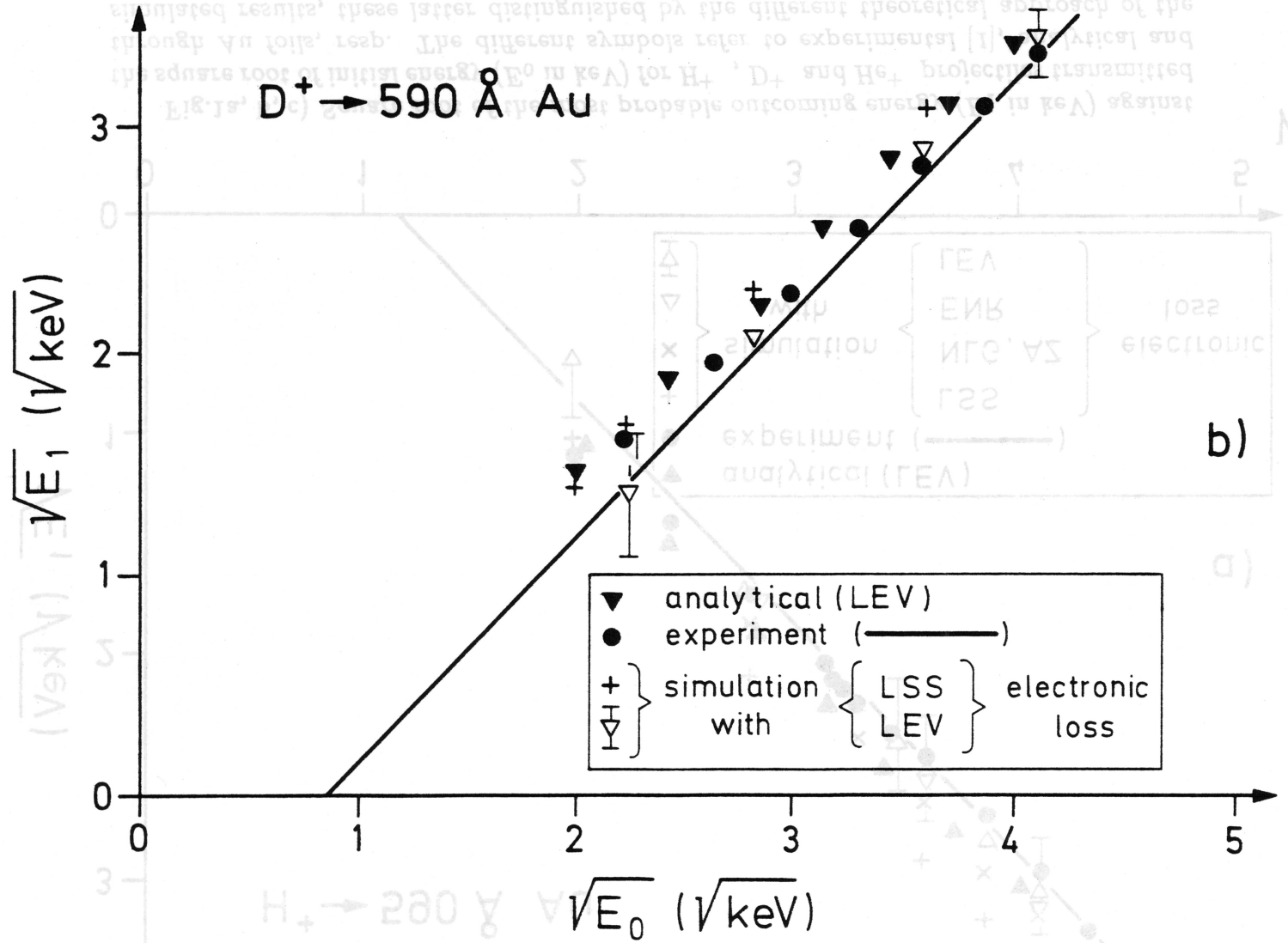
D+ → 590 Å Au
b)
analytical (LEV)
experiment (——)
simulation with { LSS, LEV } electronic loss
$\sqrt{E_1}$ ($\sqrt{keV}$)
$\sqrt{E_0}$ ($\sqrt{keV}$)
0
1
2
3
4
5

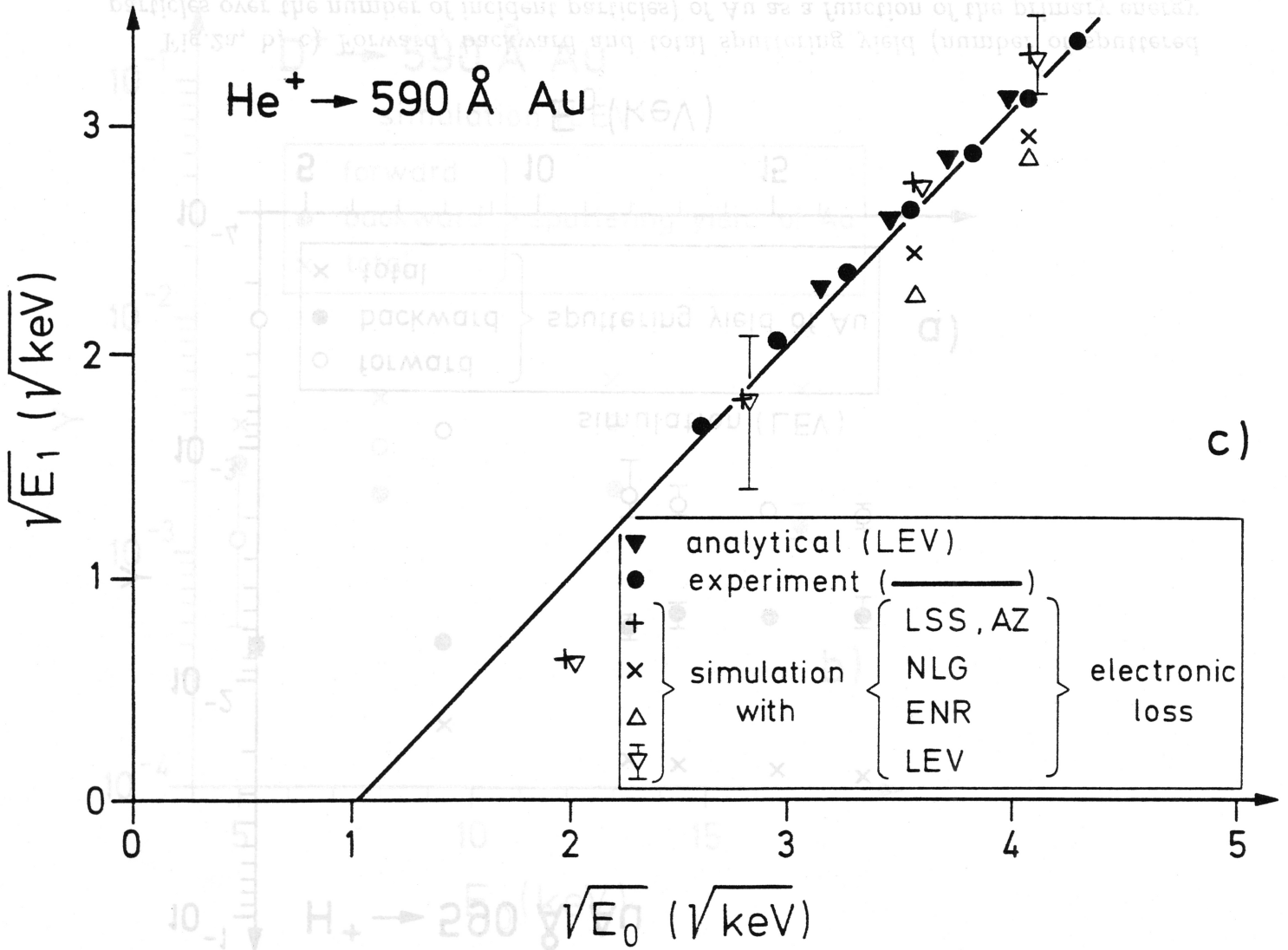
He+ → 590 Å Au
c)
analytical (LEV)
experiment (——)
simulation with
LSS, AZ
NLG
ENR
LEV
electronic loss
√E1 (√keV)
√E0 (√keV)
0
1
2
3
4
5

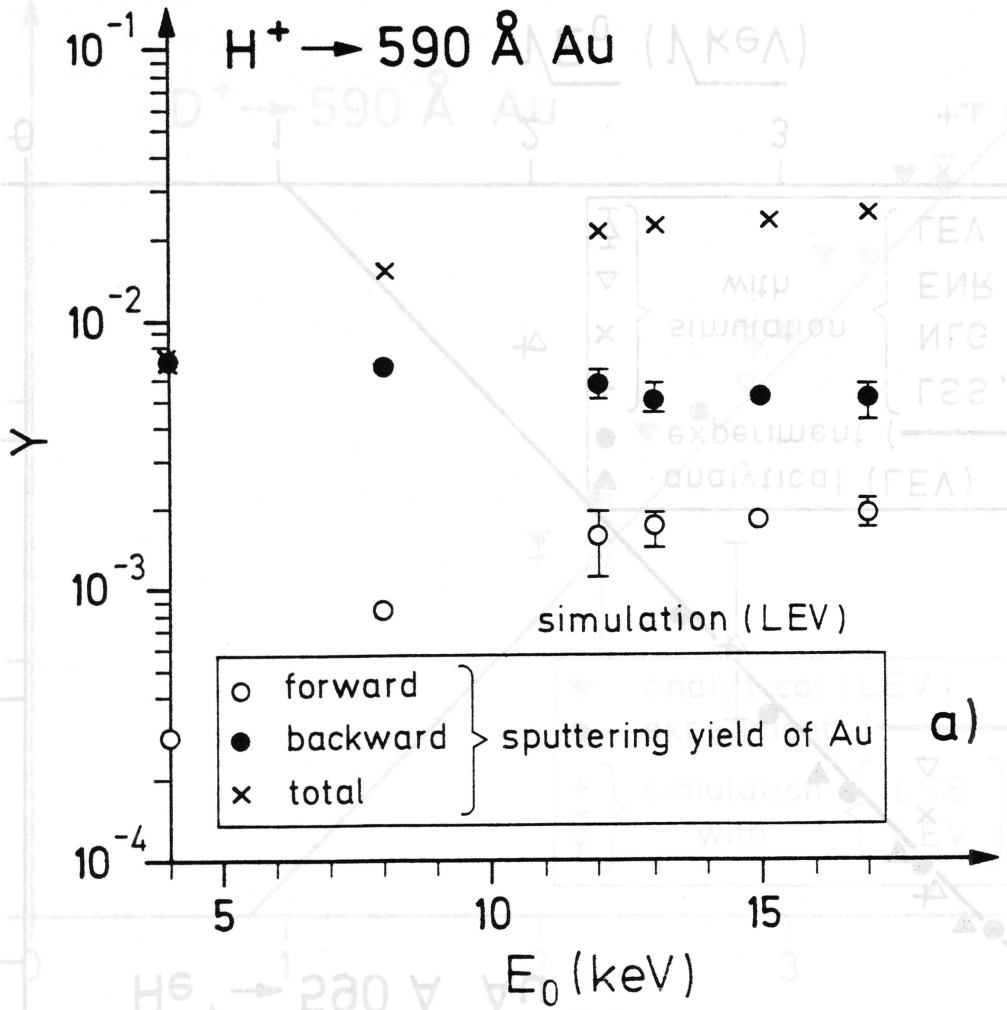

Fig.2a, b, c) *Forward, backward and total sputtering yield (number of sputtered particles over the number of incident particles) of Au as a function of the primary energy (in keV) for* H^+ , D^+ *and* He^+ *bombardment, resp. Simulation was done via LEV approach for the electronic stopping.*

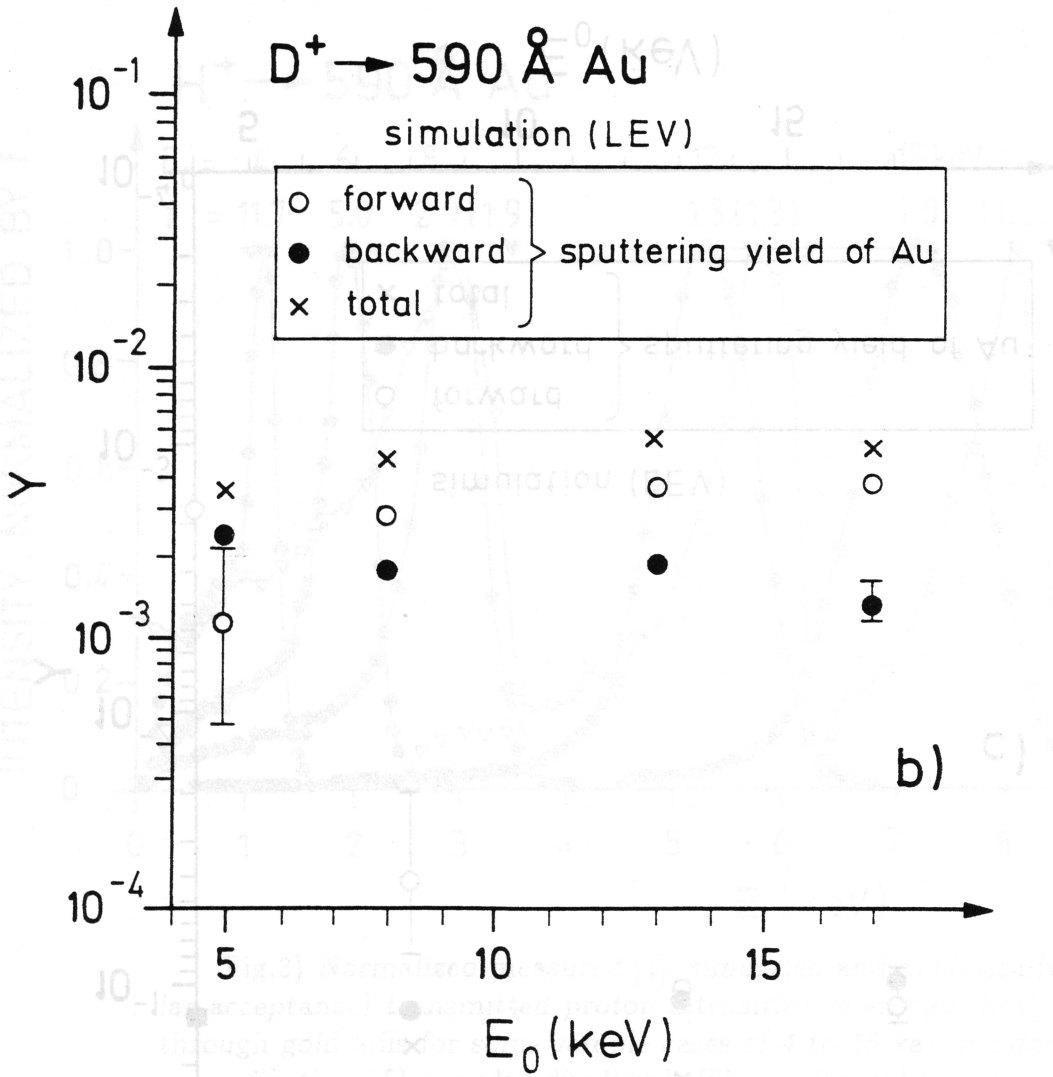
D+ → 590 Å Au
simulation (LEV)
forward
backward
total
sputtering yield of Au
Y
10-1
10-2
10-3
10-4
5
10
15
E0 (keV)
b)

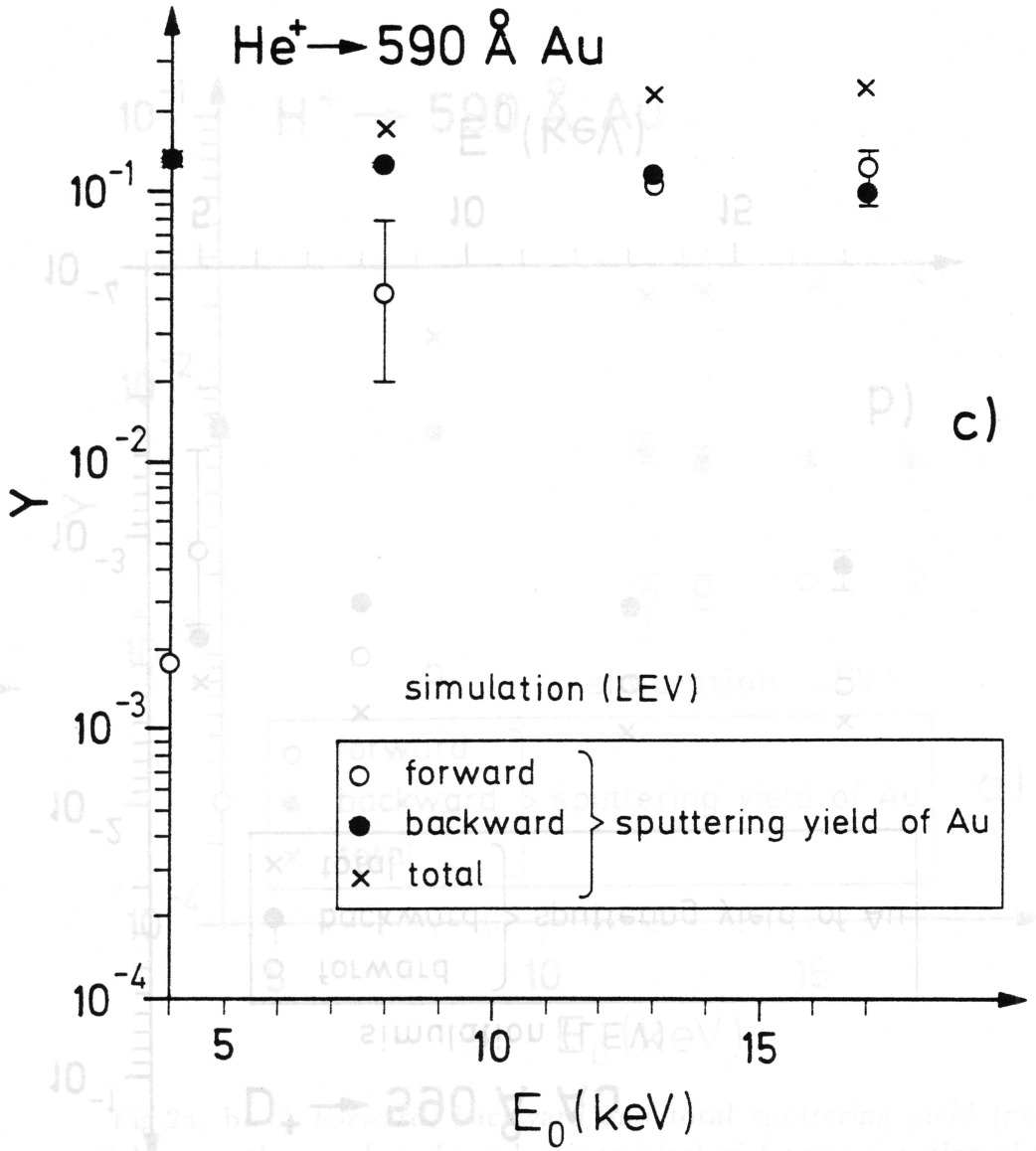
He+ → 590 Å Au
c)
Y
10^-1
10^-2
10^-3
10^-4
5
10
15
E0 (keV)
simulation (LEV)
forward
backward
total
sputtering yield of Au

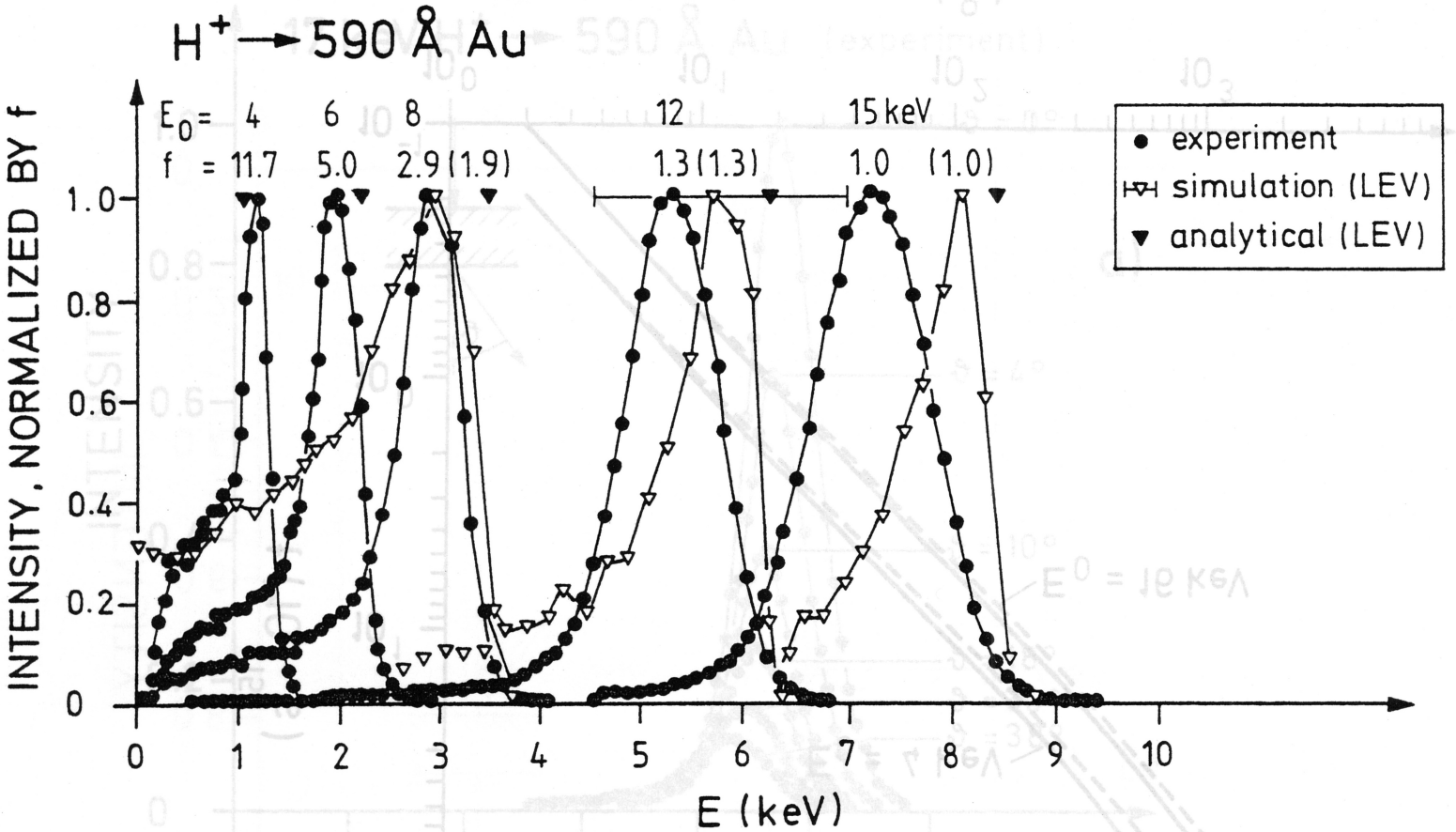

Fig.3) *Normalized measured [1], simulated and analytically determined (small angular acceptance) transmitted proton intensities vs energy (keV) of transmitted projectiles through gold foils for some sample cases of 4 to 15 keV incident energies. The factors of normalization (f) are also displayed. The horizontal bar shown as an example at the 12 keV peak shows the influence of the allowed 20 % tolerance in the foil thickness measurement. (A shift towards lower energies corresponds to thicker target.) Simulated data were obtained via LEV approach for the electronic loss. The measured 12 and 15 keV spectra are not drawn consistently with Fig.1a (taken over unchanged from [1]).*

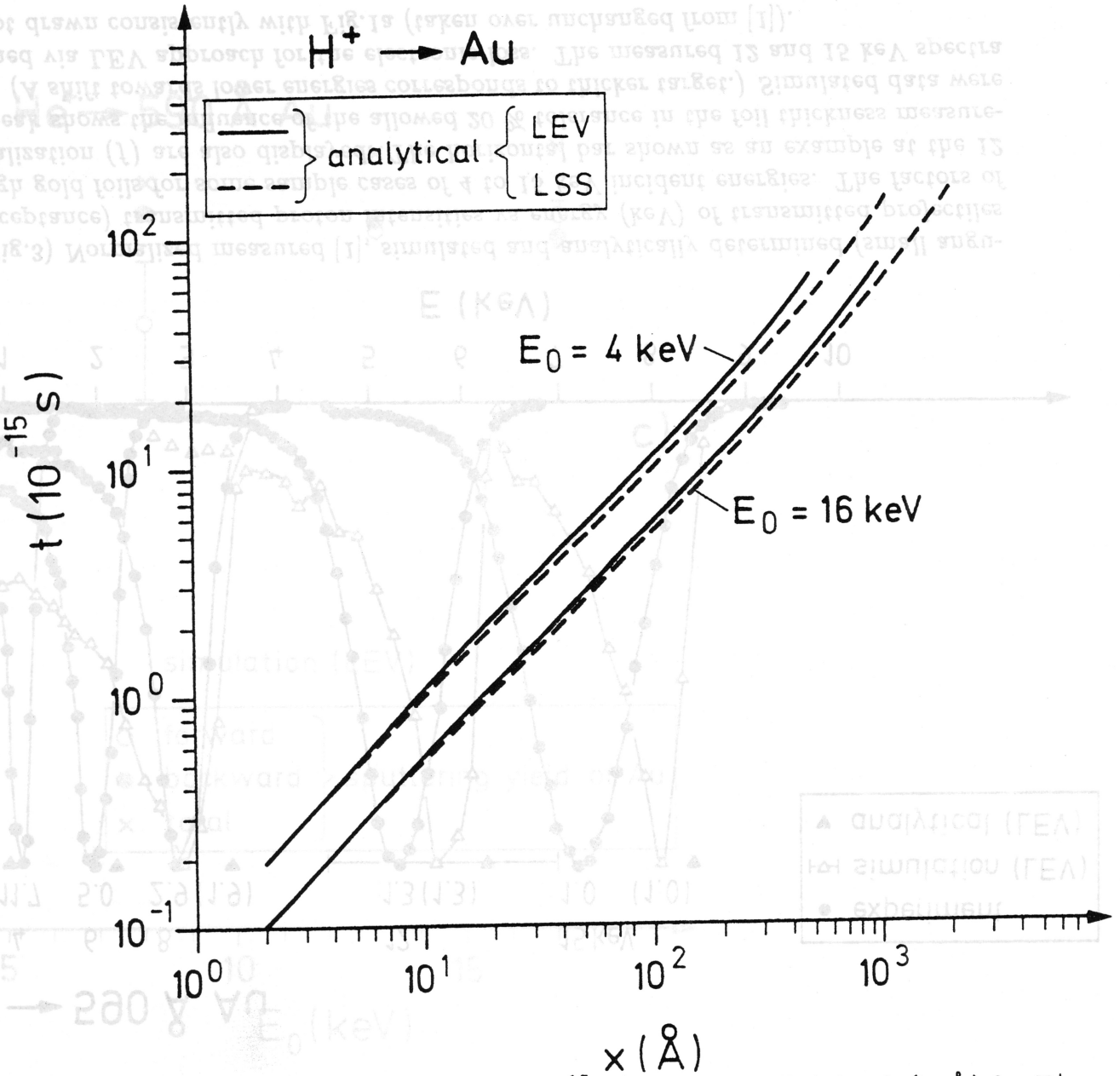

Fig.4) *Time of flight in units of* 10^{-15} *s against travelled depth (in Å) for* H^+ *penetrating in gold for 4 and 16 keV initial energies and LEV (solid line) and LSS (dashed line) coefficients of electronic stopping. Analytical calculation was done with linearized nuclear stopping.*

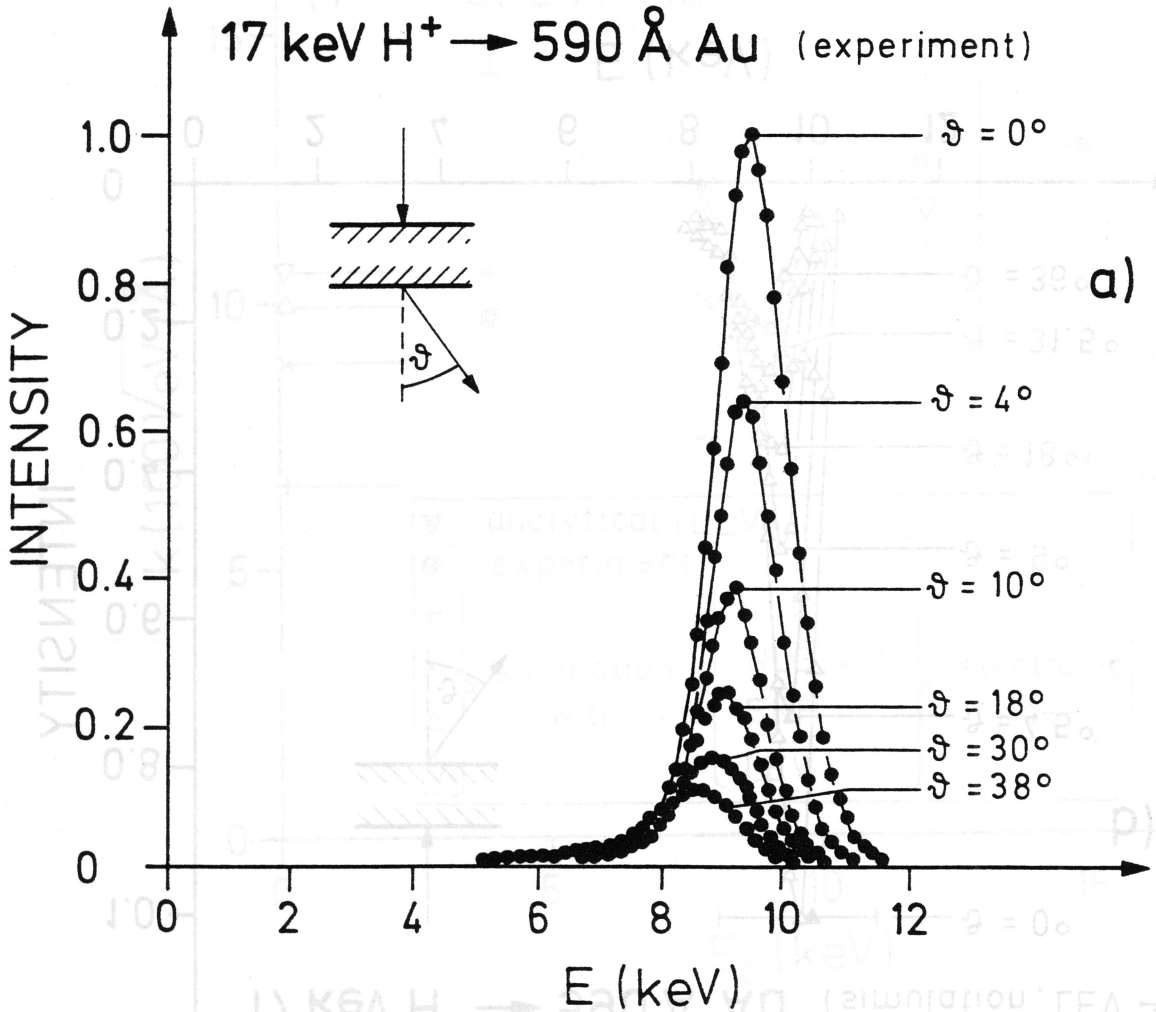

Fig.5a, b) *Normalized transmitted energy spectrum (number of transmitted particles over the number of incident particles) of 17 keV protons as measured [1], simulated and analytically determined via LEV approach, resp. parametrized by the emission angle shown in the insert. The bar shows the uncertainty due to the inaccuracy of the thickness measurement. (Lower energy corresponds to thicker target.)*

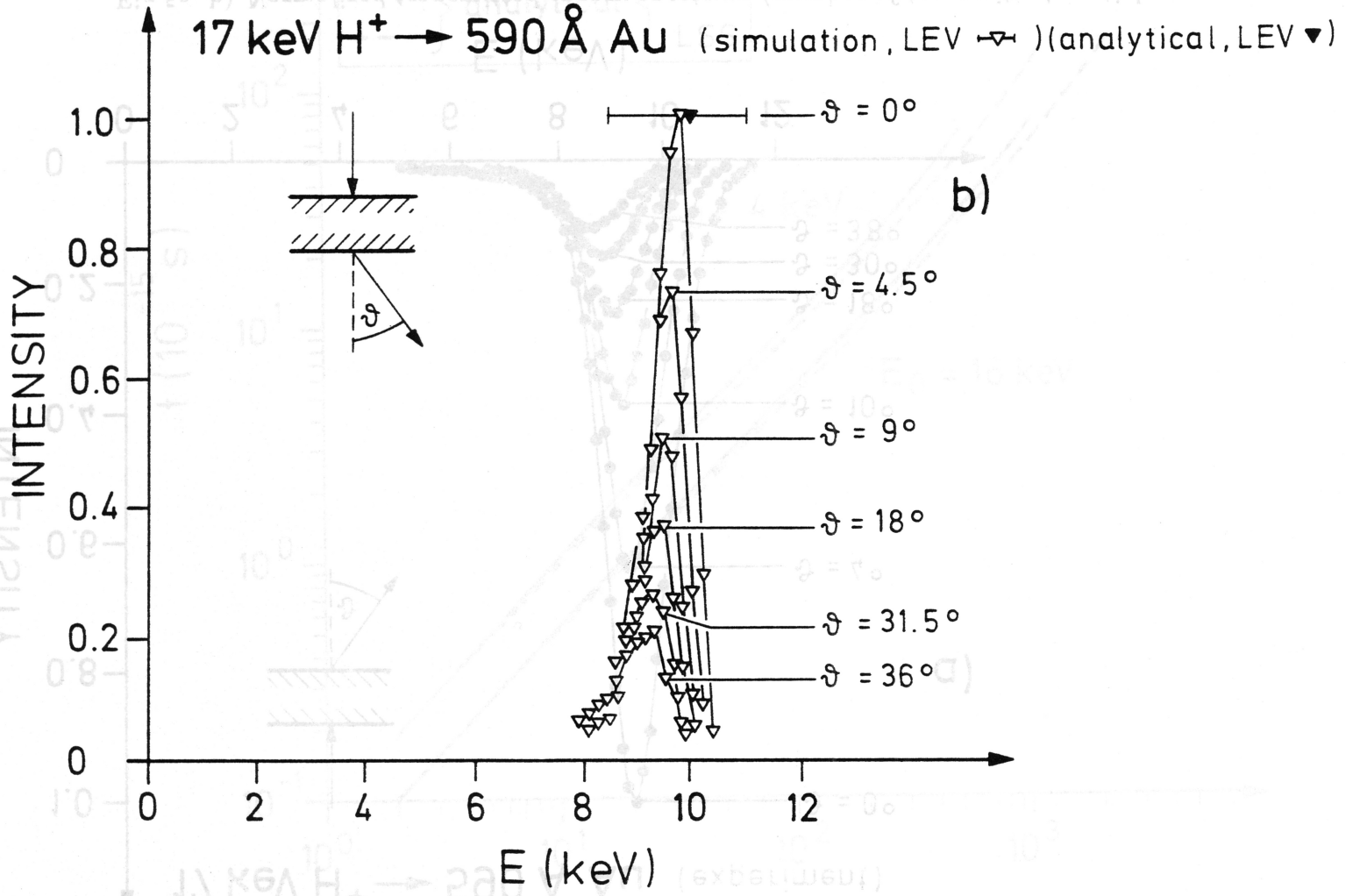
17 keV H+ → 590 Å Au (simulation, LEV ⊸)(analytical, LEV ▼)
INTENSITY
E (keV)
ϑ = 0°
ϑ = 4.5°
ϑ = 9°
ϑ = 18°
ϑ = 31.5°
ϑ = 36°
b)

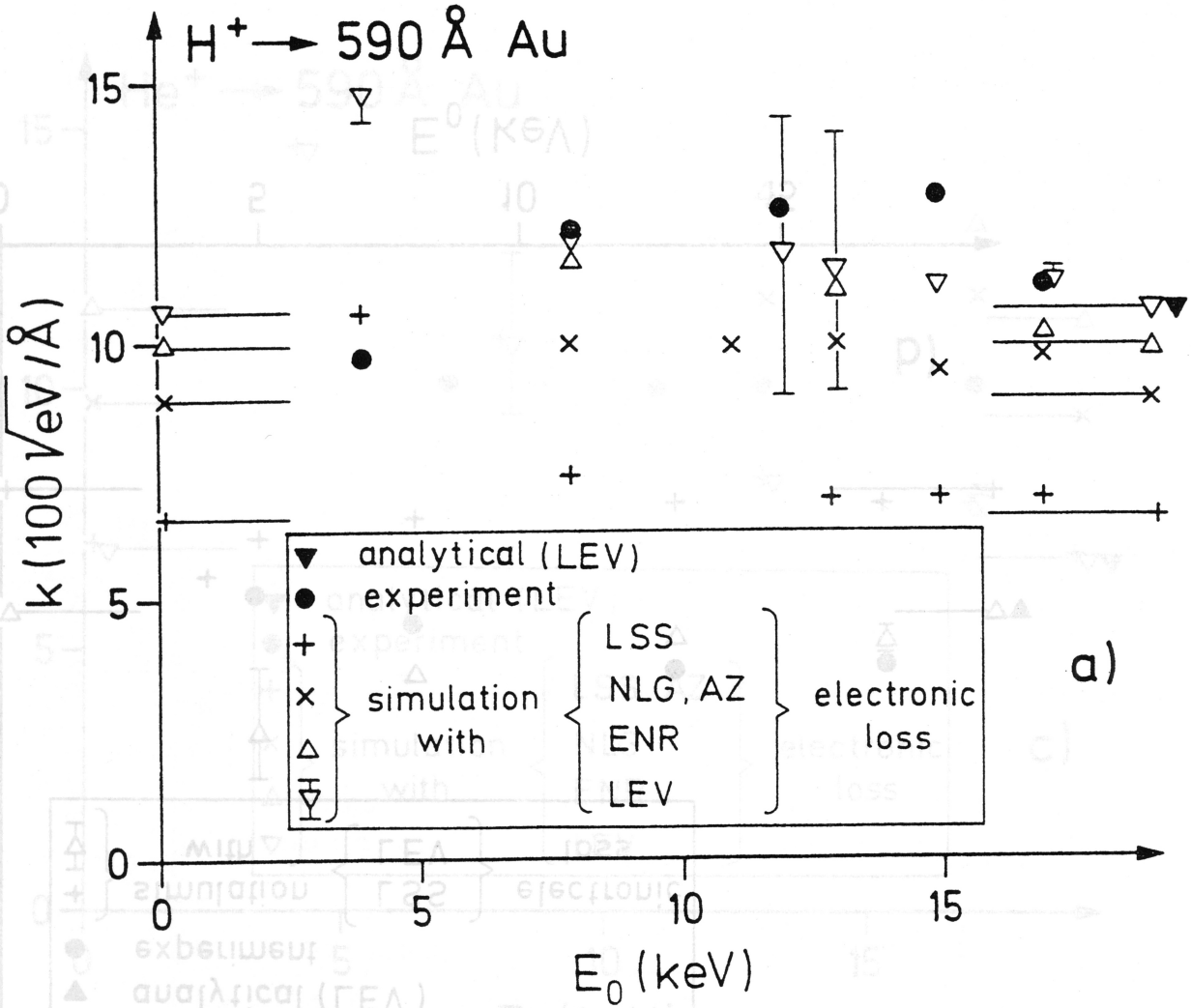

Fig.6a, b, c) *k values (in units of* $eV^{1/2}Å^{-1}$*) as a function of initial energy (keV) for* H^+ *,* D^+ *and* He^+ *projectiles transmitted through Au foils, resp. Different symbols denote different theoretical approximations for the input k values as described in the Tools section. Besides the output constants the corresponding input k 's are also illustrated by the horizontal lines.*

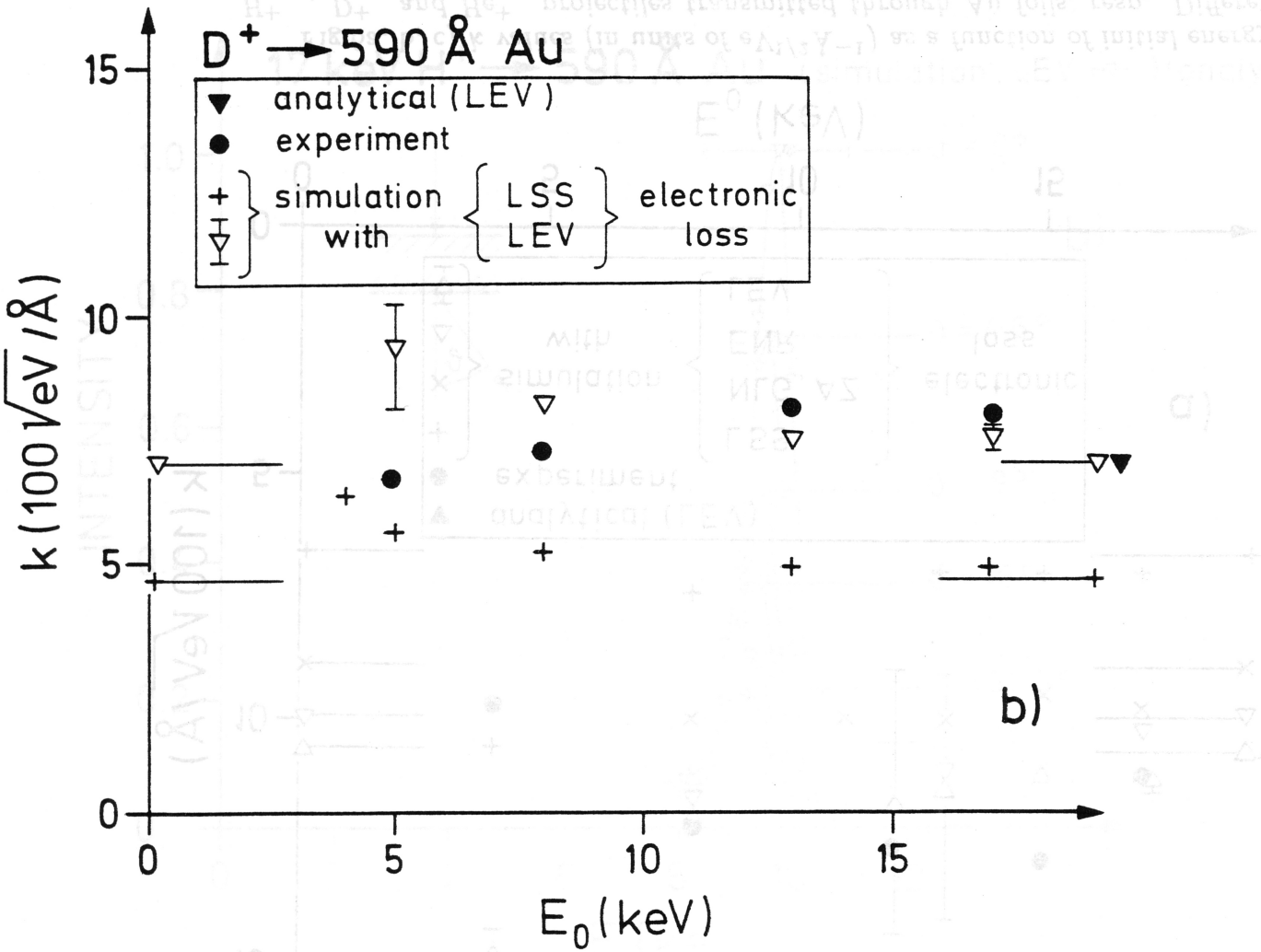
D+ → 590 Å Au
analytical (LEV)
experiment
simulation with
LSS
LEV
electronic loss
k (100 √eV / Å)
E0 (keV)
b)
0
5
10
15

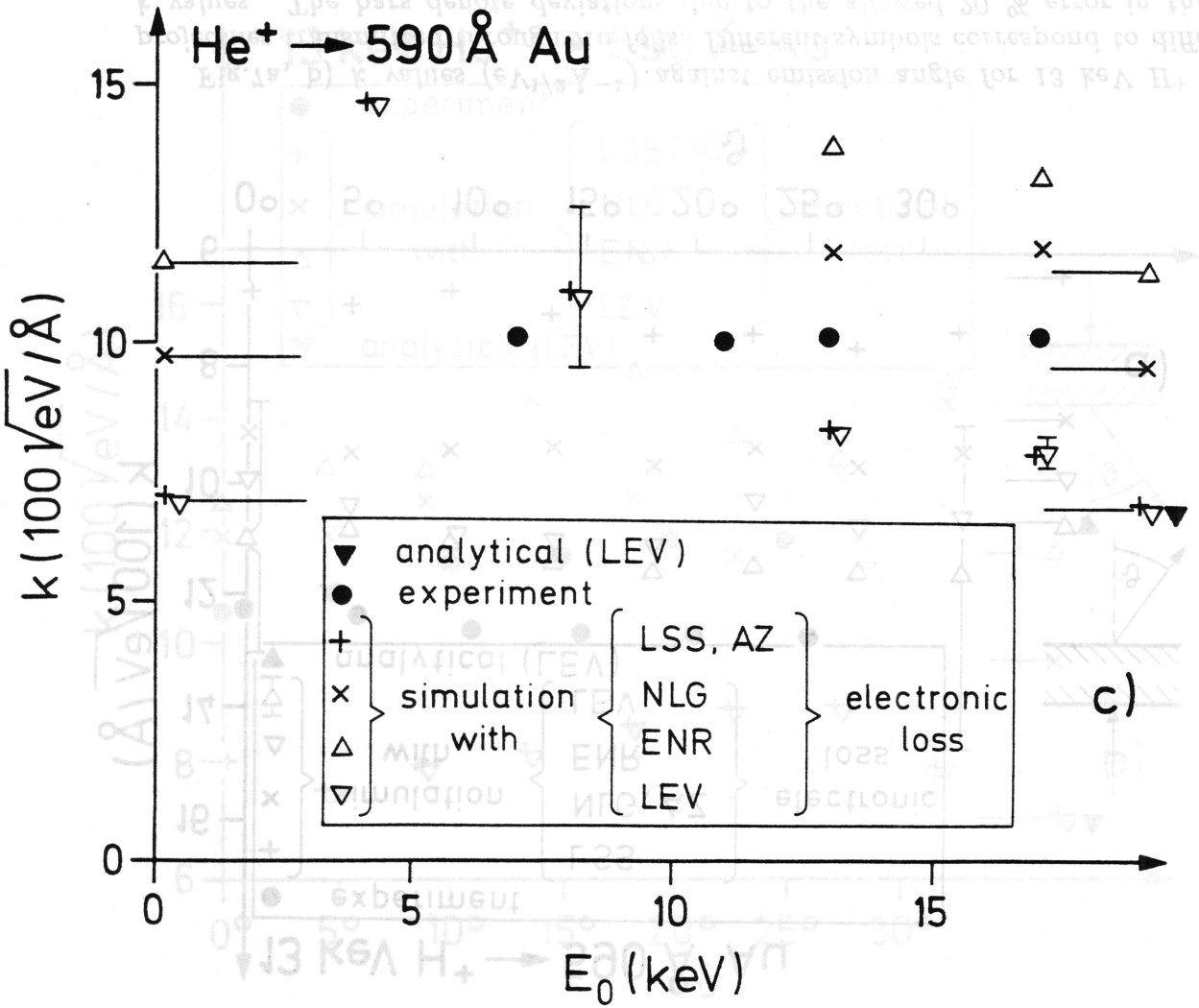
He+ → 590 Å Au
k (100 √eV/Å)
15
10
5
0
0
5
10
15
E0 (keV)
analytical (LEV)
experiment
simulation with
LSS, AZ
NLG
ENR
LEV
electronic loss
c)

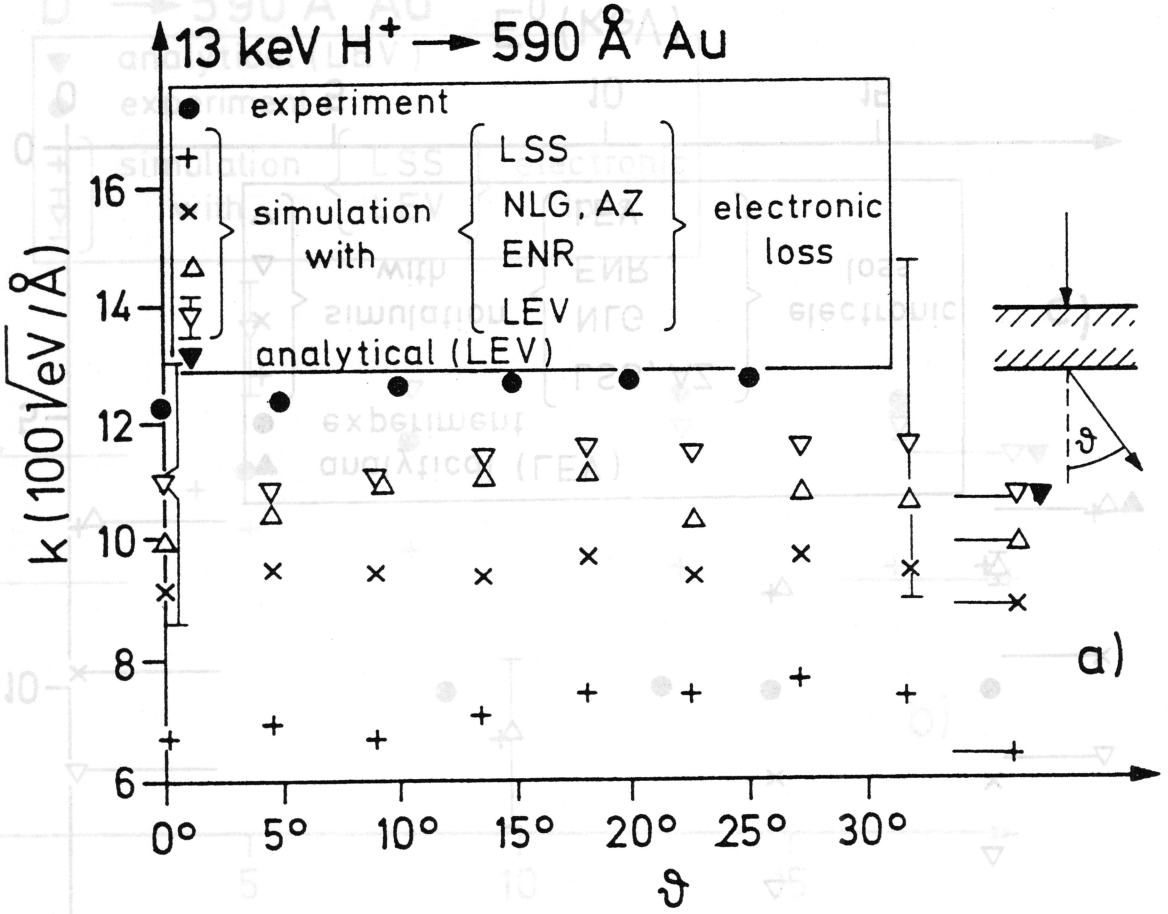

Fig.7a, b) *k values* ($eV^{1/2}Å^{-1}$) *against emission angle for 13 keV* H^+ *and* He^+ *projectiles transmitted through Au foils. Different symbols correspond to different input k values. The bars denote deviations due to the allowed 20 % error in the thickness measurement (lower k attributed to thinner target). These k values are corrected for the different pathlengths of the transmitted projectiles* [1].

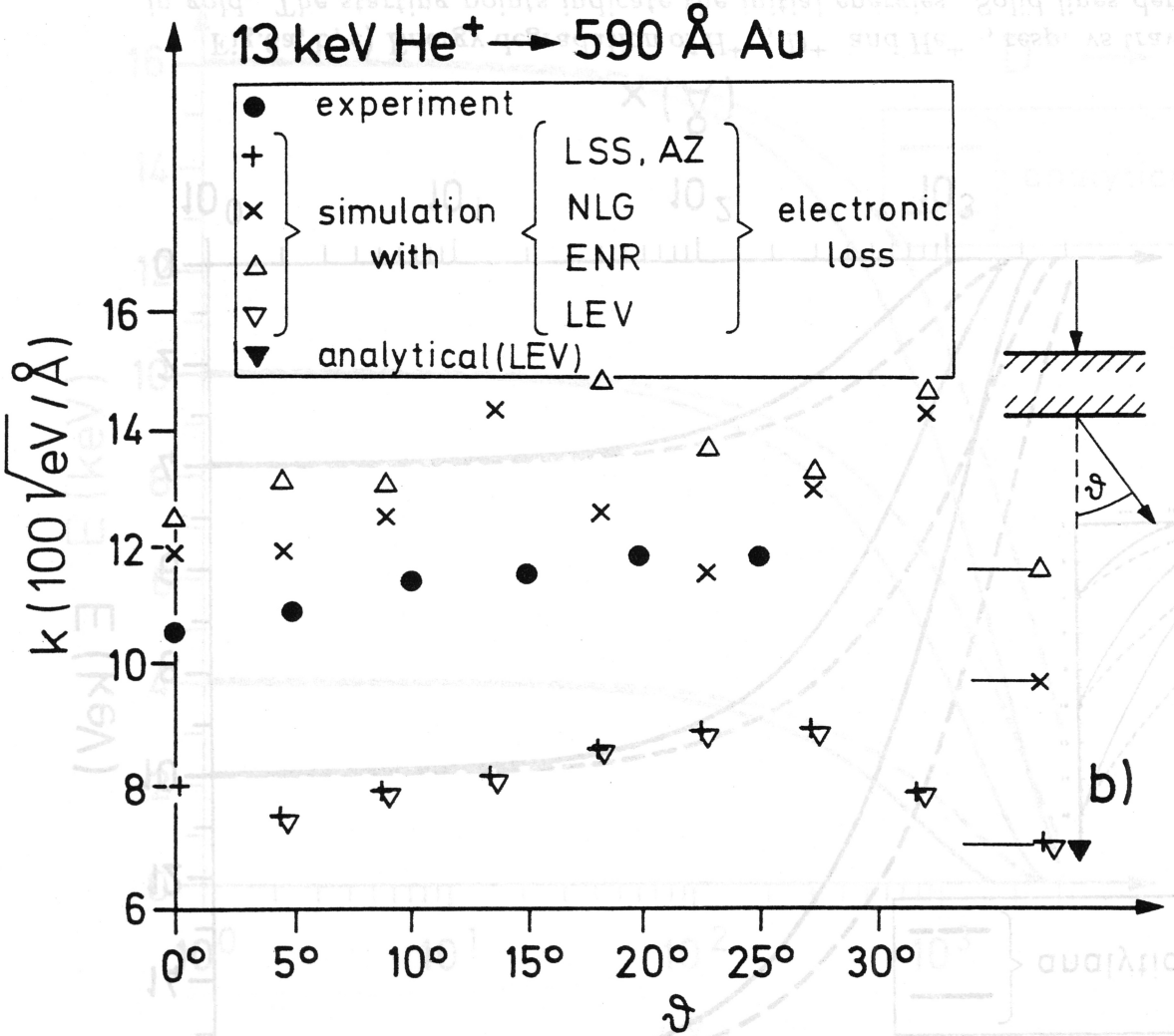
13 keV He+ → 590 Å Au
experiment
simulation with
LSS, AZ
NLG
ENR
LEV
electronic loss
analytical (LEV)
k (100 √eV/Å)
16
14
12
10
8
6
0°
5°
10°
15°
20°
25°
30°
ϑ
b)

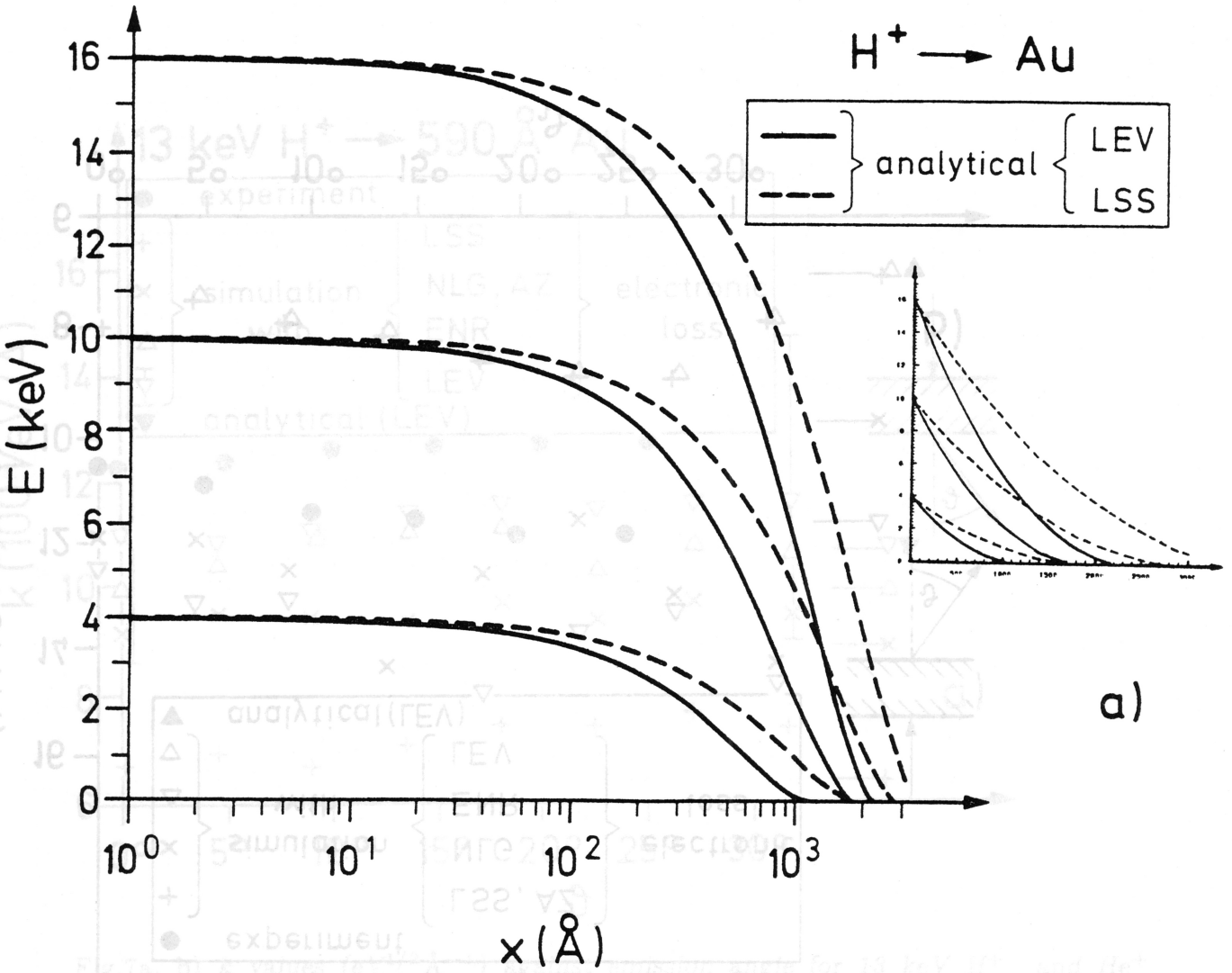

Fig.8a, b, c) *Energy degradation of H^+, D^+ and He^+, resp. vs travelled pathlength in gold. The starting points indicate the initial energies. Solid lines denote results with LEV coefficient of electronic stopping, dashed lines are attributed to other coefficients (LSS for H^+ and D^+ and ENR for He^+). The analytical calculation was done with full nuclear stopping.*

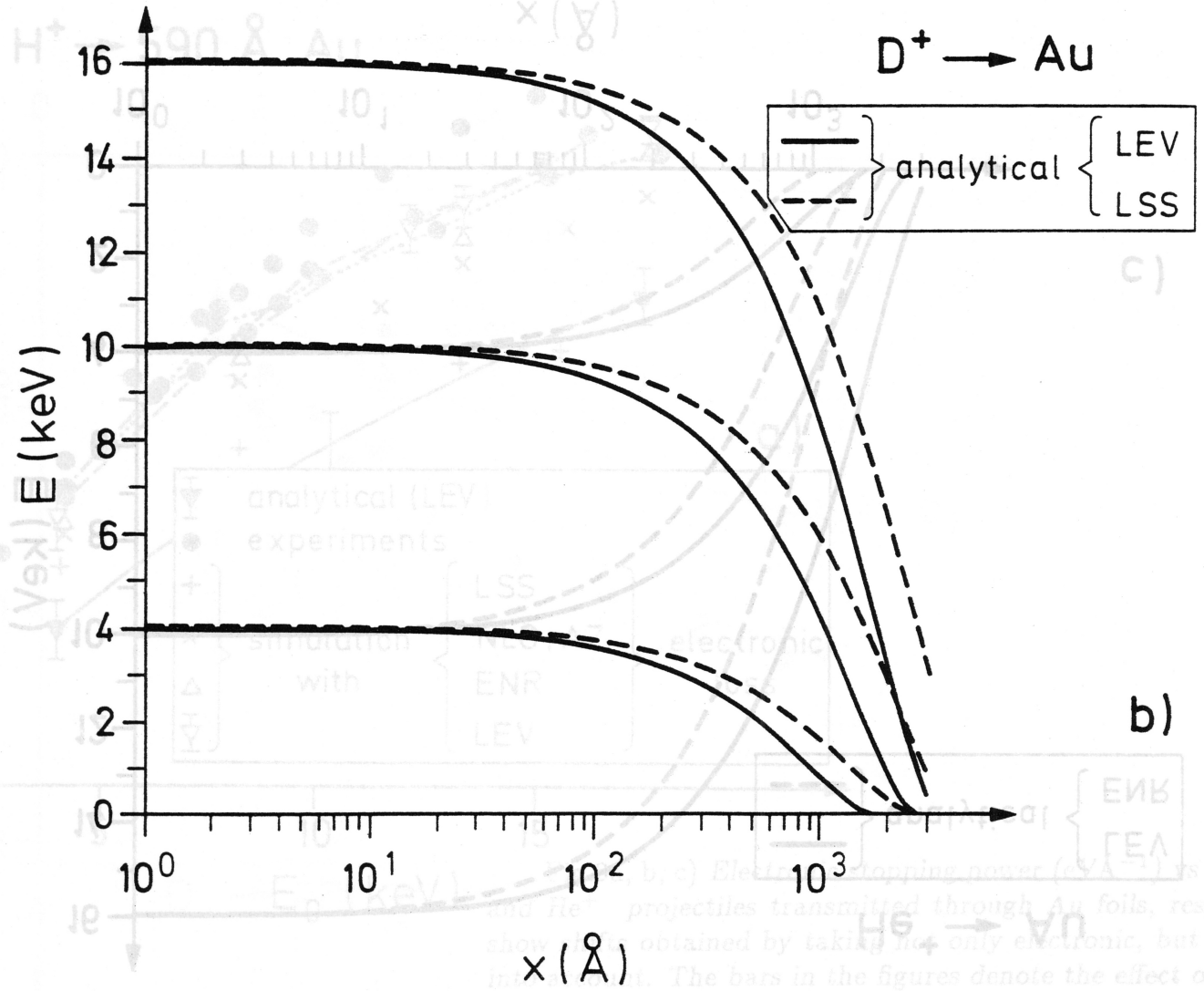
D+ → Au
analytical
LEV
LSS
E (keV)
x (Å)
b)

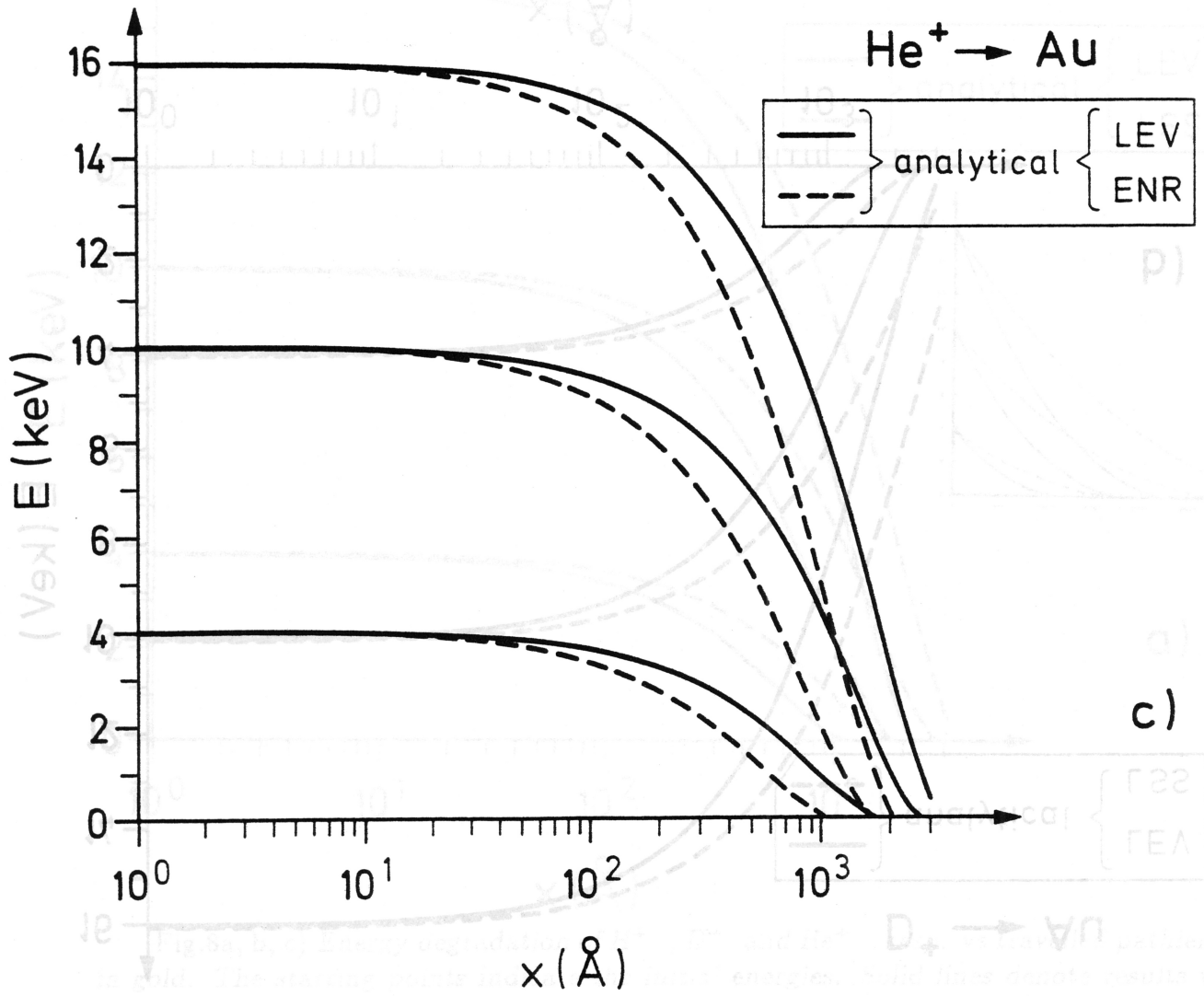
He+ → Au
analytical
LEV
ENR
E (keV)
x (Å)
16
14
12
10
8
6
4
2
0
10^0
10^1
10^2
10^3
c)

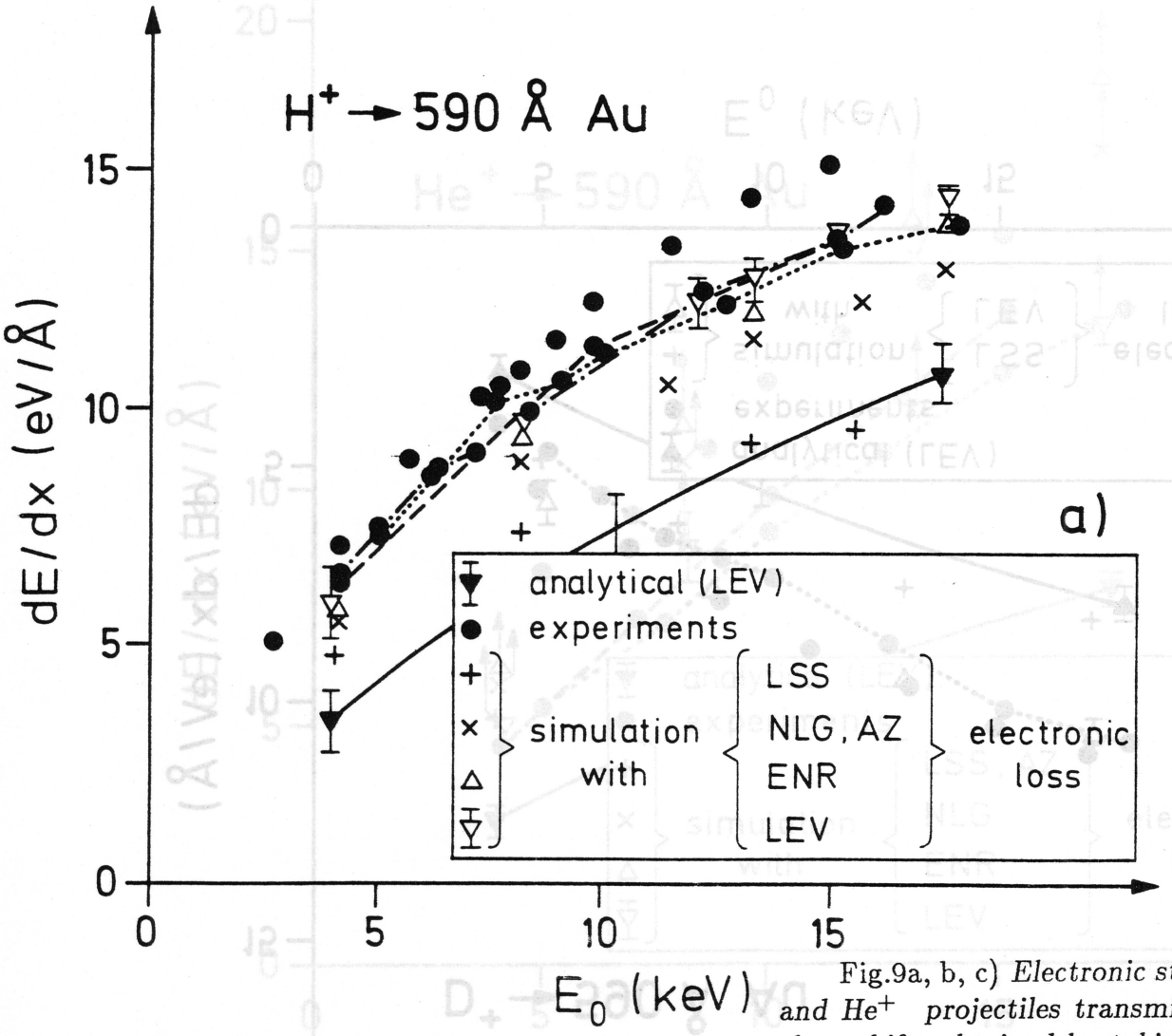

Fig.9a, b, c) *Electronic stopping power ($eV Å^{-1}$) vs initial energy (keV) for H^+ , D^+ and He^+ projectiles transmitted through Au foils, resp. The upward arrows in Fig.9c show shifts obtained by taking not only electronic, but nuclear energy loss contributions into account. The bars in the figures denote the effect of uncertain foil thickness (smaller stopping power corresponds to thinner target). Besides transmission experimental points [1] (unconnected dots), data deduced from kinetic secondary electron yield measurements [16,17,18] (dots connected by dashed, dashed-dotted and dotted lines, resp.) are also displayed. Analytical calculations were carried out with LEV electronic and full nuclear stopping.*

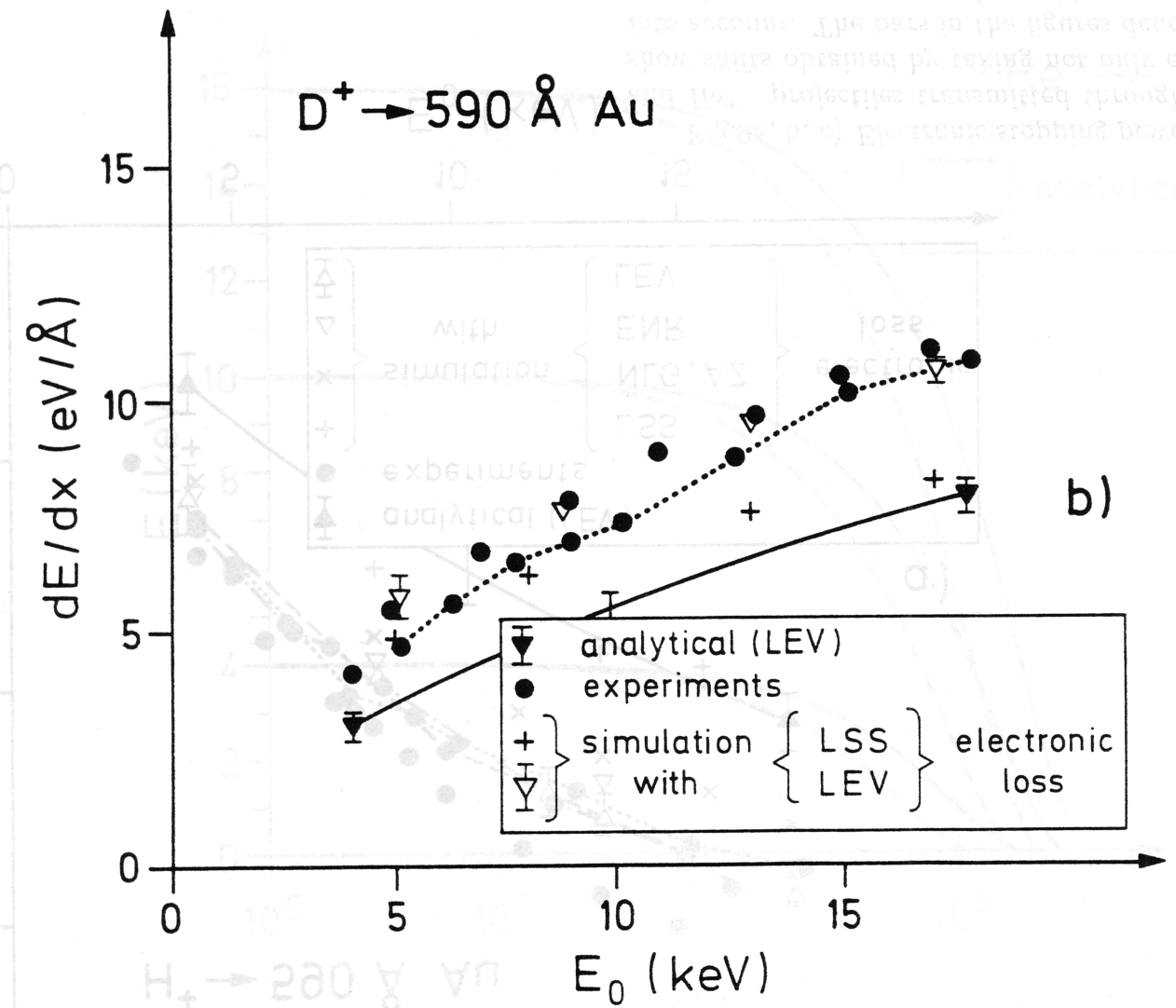
D+ → 590 Å Au
dE/dx (eV/Å)
E0 (keV)
0
5
10
15
b)
analytical (LEV)
experiments
simulation with
LSS
LEV
electronic loss

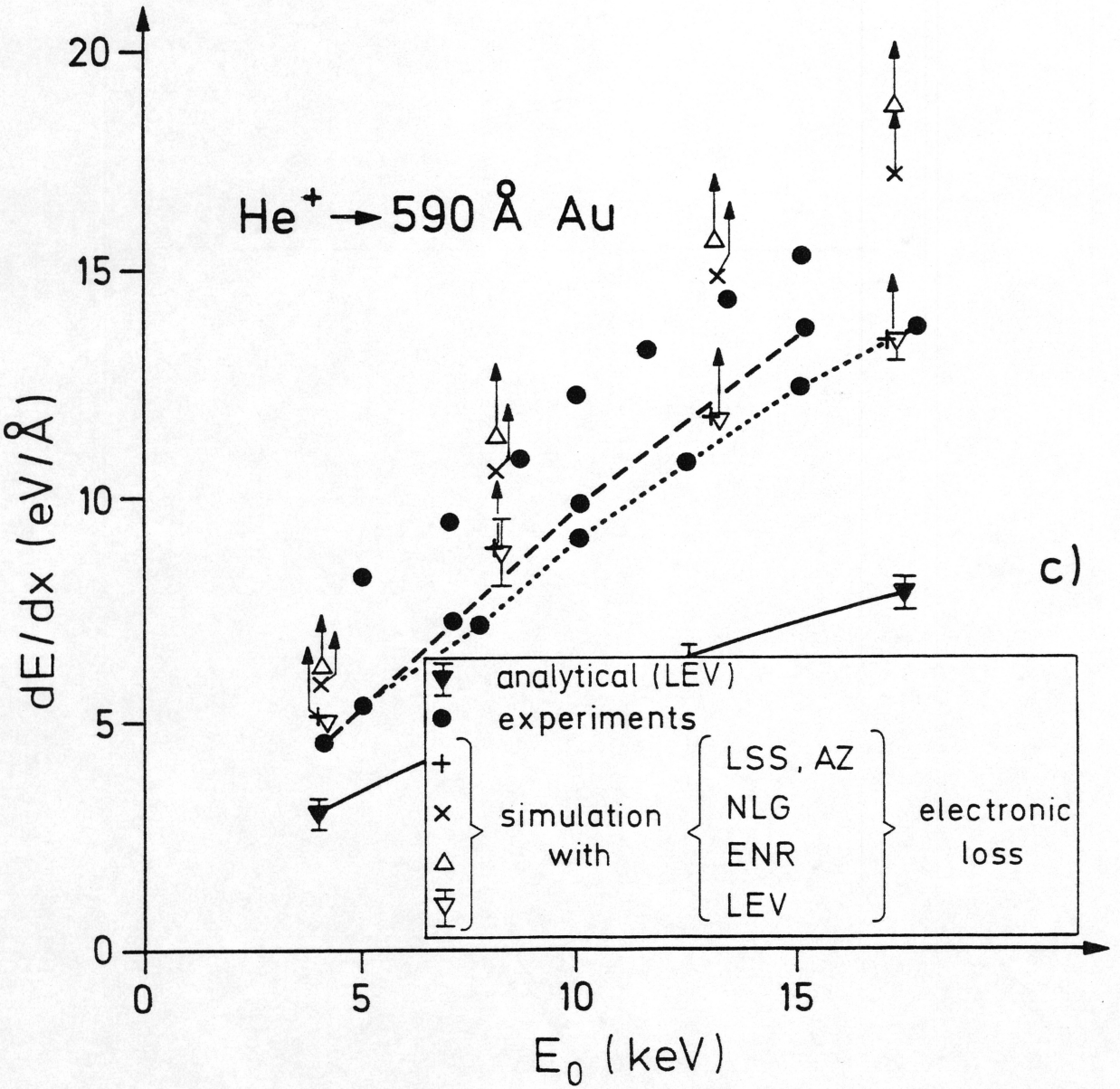
He+ → 590 Å Au
c)
dE/dx (eV/Å)
E0 (keV)
0
5
10
15
20
analytical (LEV)
experiments
simulation with
LSS, AZ
NLG
ENR
LEV
electronic loss